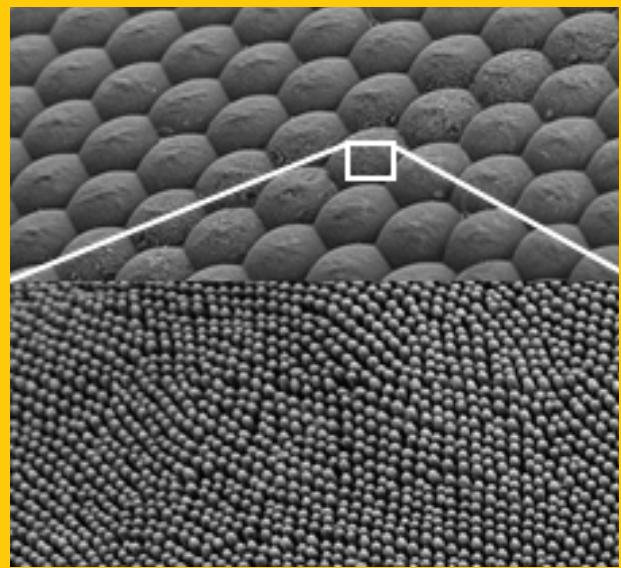


Abstract In nature, optical structures in the subwavelength range have been evolved over millions of years. For example, in the form of ‘moth-eye’ structures they show a strong anti-reflective effect on the compound eyes of night-active insects and therefore offer a successful protection over predators. In this contribution the advantages and challenges to transfer this natural concept of subwavelength structured optical interfaces to high-end optical systems are discussed. Here, in comparison to alternative conventional multilayer systems, the bioinspired anti-reflective structures offer a wide wavelength range and a broad angle dependency. Additionally, adhesion problems are reduced drastically. Simultaneously to the theoretical consideration of the best profile form of the subwavelength structures, appropriate realization technologies have been developed in recent years, where both top-down and bottom-up approaches have been investigated. Depending on the choice of the structuring technique, anti-reflective subwavelength structures are applicable to a wide spectrum of optical elements ranging from micro-optical components to aspheres for applications in imaging and also illumination setups of high-end optical instruments.



Lessons from nature: biomimetic subwavelength structures for high-performance optics

Robert Brunner^{1*}, Oliver Sandfuchs², Claudia Pacholski³, Christoph Morhard³, and Joachim Spatz^{3,4}

1. Introduction

Regarding the progress of optical science and technology over the years and centuries, which were leading to new optical working principles and new optical components, one finds that most often the basic physical ideas were already evolved in nature over millions of years.

Today, the ideas of bionics have intruded into many technological fields, c. f. [1]. For one aspect, bionics provides a huge pool of systematical solutions that were created in the natural process of evolution (principles of evolution of the first kind [2]).

The variety of biomimetic concepts include the following selected optical examples:

- Catadioptric systems in the combination of imaging mirrors and classical (refractive) lenses, which allow the minimization of chromatic aberrations in imaging systems such as microscopes, photolenses or high-end lithography optics for semiconductor manufacturing industry [3], are also found in scallop eyes [4].
- Multilayer structures creating the reflecting surface of the extreme-UV optics introduced for the next-generation lithography at 13 nm in semiconductor industry [5] rely on the identical physical principle as the coating of the cornea of the facets from the eye of a horsefly [6].
- Photonic crystals, three-dimensional structures of alternating high and low refractive indices and a periodicity in the wavelength range, show a photonic bandgap, which means that a specific wavelength range is not allowed to propagate. Today, artificial ‘photonic-crystal fibers’ are manufactured for application in illumination systems. But also in nature, ‘photonic-crystal fibers’ were identified, e. g., in a sea mouse, a marine worm with the appearance of an iridescent mouse [7]. Colors on butterfly wings and beetle shells are also engendered by photonic nanostructures [8].
- A last example of bioinspiration in recent years is the concept of deformable refractive surfaces, which was transferred to liquid lenses, allowing focusing and zooming in artificial optical systems [9–11]. This resembles the accommodation mechanism of the eyes of reptiles,

¹ University of Applied Sciences Jena, Carl Zeiss Promenade 2, 07745 Jena, Germany ² Microstructured Optics, Carl Zeiss Jena GmbH, Carl-Zeiss-Promenade 10, 07740 Jena, Germany ³ Max Planck Institute for Intelligent Systems (formerly: MPI for Metals Research), Heisenbergstr. 3, 70569 Stuttgart, Germany ⁴ University of Heidelberg, Im Neuenheimer Feld 253, 69120 Heidelberg, Germany

* Corresponding author: e-mail: Robert.Brunner@fh-jena.de

birds and mammals, which is based on deformable eye lenses. Yet, a complete technical replica of the human eye – including a suitable muscular-like actuation – still remains a tremendous technological challenge.

Bionics in the 21st century has reached a second level of technological relevance. It has been realized that nature not only provides a pool of self-optimized solutions, such as the examples mentioned above, it also supplements the way to get there, i. e. bionics provides a pool of self-optimized technological processes [12].

Here, effective optimization processes are based on the principle of self-organization, which nowadays is considered to be one of the evolutionary principles of the second kind [1], and, without it, the evolutionary principles of the first kind would have not been successful.

Both principles, the transfer of an optical solution found in nature into man-made optical systems and also the implementation of self-organization processes into manufacturing technologies, are followed impressively in the context of ‘moth-eye structures’, a subwavelength structure found on the cornea of night-active insect, allowing a strong antireflection (AR) effect [13].

The discovery of these subwavelength structures was made 1967 by Bernhard [14]. He proposed that the anti-reflective property of this subwavelength structure is based on an effective graded transition of the refractive index between the air and the cornea. In 1973 Clapham and Hutley [15] proved this for the visible wavelength range: The wavelength of the incident light is too large to resolve the fine surface structure and the subwavelength structured interface is optically equivalent to an unstructured film whose optical properties vary with profile depth.

This AR effect offers a vital competitive advantage in two ways: first, more light reaches the optical receptors, which increases the effective light detection at night. Secondly, and more important, reflections from the moth’s eyes are suppressed and the moth is less visible to its predators.

Figure 1 shows scanning electron microscope images of a typical moth eye [16]. At low magnification (upper image) the hexagonal array of the facets of the compound eye becomes clearly visible. With increasing magnification (lower part) an area covered with conical and uniform protuberances is observable. The diameter of each protuberance is about 100 nm and the spatial periodicity is approximately

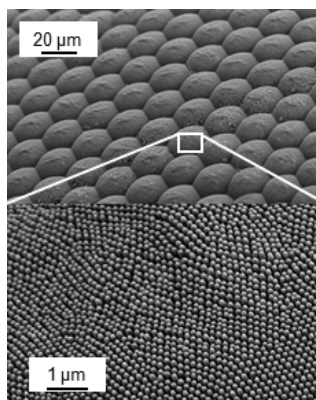


Figure 1 Scanning electron microscopy images of a night-active insect. The upper part shows the hexagonal structure of the compound eye. With increased magnification (bottom part) a subwavelength periodic surface corrugation becomes visible [16].

170 nm, which is well below the wavelength of the visible spectrum.

The efficient anti-reflective property of the moth-eye structures can be tracked back millions of years in the evolution. For example, moth-eye structures are discovered on the eye of a dolichopodid fly, preserved in 45 million year old Baltic amber [17].

The transmission efficiency of light through an optical component is also crucial to many technical optical systems. Fresnel reflections occur at an optical interface between two media. A major part of the light is transmitted and the residual part is reflected. Despite some applications, such as interferometer objectives, where the Fresnel reflections are used for lens-quality testing [18], Fresnel reflections are a disadvantageous effect for most optical applications and reduce the light efficiency of the optical system at each optical interface.

Today, most frequently antireflection coatings are based on multilayer interference structures with alternating high and low refractive indices. Beyond multilayered structures, the biomimetic optical concept of the moth eye and effective media has been transferred to the technological world within the past decades. Shortly after their discovery in the 1970s, artificial moth-eye structures were investigated for applications as solar selective absorbers [19, 20]. In the 1980s and 1990s, the research focus was set more onto the basic characteristics of effective media than to the concrete application scenarios. In this age, the basic characteristics of the effective media, such as birefringent artificial dielectrics [21–23], polarization sensitive elements [24–26] or blazed gratings and lenses [27–31] were investigated. The interest in subwavelength gratings was also driven by the new possibilities of numerical simulation and of micro- and nanofabrication.

In the first decade of the new century the focus returned more and more onto industrial applications of subwavelength structures for guided-mode resonant grating filters [32], microlenses for the infrared spectral region [33], e. g., as well as onto new aspects of more refined fabrication techniques, such as self-assembled structures by colloidal crystals [34] and stochastic antireflection structures on polymer surfaces by plasma treatment [35].

For applications as AR surfaces it was found that different characteristics of subwavelength structures are advantageous compared to stacks of thin dielectric films. For example, thin-film coatings may suffer from adhesion problems, especially when the thermal expansion coefficients of substrate and layer material are different and the optical devices are used over a broad thermal range. Additionally, due to the restrictions in thin-film coating materials, the available number of discrete refractive indices is also limited. A further aspect concerns the sensitivity of the reflectance in dependence of incident angle or wavelength. Here, in general, a subwavelength AR structure tolerates more variations in comparison to simple layer configurations.

Based on these characteristics and, additionally, to their potential of mass production via relatively simple replication processes such as hot embossing, injection molding or UV curing, the application of moth-eye structures as AR coatings is always regarded as commercially attractive.

In the late 1990s, several commercial applications started. Large-area applications, in particular, were based on the work at the Fraunhofer ISE [36]. At that time, the company Fresnel Optics [37] in Germany produced many thousands of Fresnel lenses for liquid-crystal projectors equipped with anti-reflective moth-eye structures. A short time later, the company Holotools [38] began to master-fabricate moth-eye structures by interference lithography on large areas of up to nearly square meters.

The technological realization of moth-eye antireflection structures is often accomplished by so-called top-down microstructuring processes, e.g [39], which means that conventional lithographic processes introduced for structuring in the micrometer range are extended to the subwavelength range. However, recent technology development does not simply copy the natural phenomenon of the moth eye but aims at a self-organized manufacturing process [40], in particular, the block-copolymer micelle nanolithography [41] or other bottom-up microstructuring processes, e.g [42]. References [43, 44] present an overview of different fabrication techniques on silicon and fused silica substrates and discuss performance aspects especially for sunlight harvesting.

2. Theoretical considerations

2.1. Specular reflection at optical interfaces

Fresnel reflection is an electromagnetic phenomenon that occurs at an optical interface between two materials of different refractive indices as a consequence of the sudden change of the refractive index at a discontinuous boundary [45].

In the simplest case for rays incident perpendicular to the surface, the reflectance is given by the reflection coefficient R , which is independent of the state of polarization [46]

$$R = \left(\frac{n_1 - n_2}{n_1 + n_2} \right)^2, \quad (1)$$

where n_1 and n_2 are the refractive indices at either side of the boundary. For the more general case of oblique incidence, the Fresnel's formulae become polarization dependent and the two reflection coefficients now yield

$$R_{\text{TE}} = \left(\frac{n_1 \cos \theta_1 - n_2 \cos \theta_2}{n_1 \cos \theta_1 + n_2 \cos \theta_2} \right)^2, \quad (2)$$

for the TE polarization, and

$$R_{\text{TM}} = \left(\frac{n_2 \cos \theta_1 - n_1 \cos \theta_2}{n_2 \cos \theta_1 + n_1 \cos \theta_2} \right)^2, \quad (3)$$

for the TM polarization, respectively. Here, θ_1 is the angle of incidence and θ_2 is the angle of refraction according to Snell's law. In the case of a series of refractive indices, the total reflectance is a result of the interference of all reflections at each incremental step along the discontinuous refractive-index gradient.

The boundary surface has to be either planar or, at least, should possess a tangential smoothness for Fresnel reflections to occur. There are two fundamental methods to avoid the effect of Fresnel reflection: first, multilayered stacks of two or more alternating optical materials [47] or, secondly, high-frequency surface-relief structures, e.g [33], or even the combination of multilayers with a few structured top layers [48].

In the first method, following thin-film theory, a single layer will exhibit minimum reflectivity at normal incidence when the reflectance from the air/film interface interferes destructively with the reflection at the film/substrate interface. This phase condition is fulfilled when the depth of the profile h satisfies:

$$h = \frac{\lambda}{4n_{\text{Layer}}}, \quad (4)$$

where λ is the wavelength of light. Additionally, a complete destructive interference will only occur if the amplitudes of both reflecting waves are identical, which implies an amplitude condition for the refractive index of the layer n_{Layer} :

$$n_{\text{Layer}} = \sqrt{n_1 \cdot n_2}. \quad (5)$$

For example, to fulfill the last equation for the interface between air ($n_{\text{air}} = 1$) and a typical inorganic glass (assumption $n_2 = 1.5$) the refractive index of the layer has to be $n_{\text{Layer}} \sim 1.22$, which is not available for thin-film materials.

A more advanced approach to layered antireflection coatings is the extension of a single layer to a multilayered thin-film stack. Here, alternating layers of high and low refractive index generate multiple beam interferences. At each interface between two adjacent layers there is partially light reflected and transmitted. As a consequence, this leads to low reflectivity for more than a single wavelength up to a broadband antireflection coating stack. Eventually, for a large number of layers, a one-dimensional photonic crystal is created [49].

While the layered solution relies on the interference of optical waves, in the second method, surface-relief gratings with high-frequency periods belong to a special class of diffractive elements, which modify the boundary between the two optical materials.

When light is incident on a diffractive element with period g the angles of the transmitted diffraction waves $\theta_{t,m}$ in the m th diffraction order are given by the grating equation:

$$\sin(\theta_{t,m}) = \frac{m\lambda}{gn_2} + \frac{n_1}{n_2} \sin(\theta_i). \quad (6)$$

Here, n_1 and n_2 are the refraction indices of the incident and the transmitting medium, θ_i the incidence angle as measured from the grating's surface normal and λ is the incident free-space wavelength. Let's assume that we have a one-dimensional sawtooth-like structure (e. g., as in Fig. 2a.). Then diffraction orders emerge and the transmitted light is

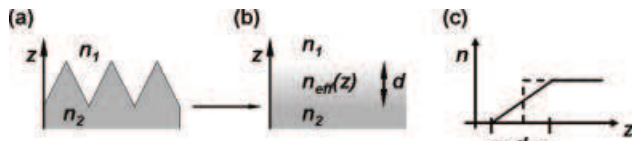


Figure 2 (a) A typical tapered antireflection structure, (b) the gradual increase of the refractive index, and (c) the corresponding evolution of the refractive index with (solid) and without (dashed) the antireflection structure as depicted in (a).

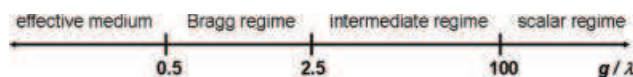


Figure 3 Schematic of fundamental diffraction regimes. The transition from one regime to the other has been indicated by approximate values of g/λ as a rough orientation.

distributed over the diffraction orders and Fresnel's formulae [45] are no longer valid. Yet, for surface structures with relatively large periods g compared to the wavelength λ of light (scalar regime in Fig. 3) the total sum of the diffracted light over all diffraction orders still equals the transmission and reflection efficiency calculated by Fresnel's formulae.

As a consequence, diffractive optical elements such as triangular blazed gratings, e. g., with large structure periods, still show Fresnel reflections, and AR coatings or even high-frequency AR structures, themselves, are needed, in addition, to suppress these reflections (see Sect. 5).

The approximation of Fresnel's formulae for microstructured surfaces holds as long as there are many propagating diffraction orders and evanescent modes do not gain considerable energy. However, as soon as the structure period is decreased, the number of diffraction orders is reduced and electromagnetic effects of diffraction beyond the scalar model become dominant.

Figure 4 shows the diffraction efficiency of a blazed grating, for which a dominant part of the light is diffracted in the +1st order (solid curve). The more the structure period is decreased the less light is diffracted into the +1st order and, eventually, more light will be diffracted into other orders because of electromagnetic shadowing effects [50]. In particular, the -1st order (dashed curve) gains energy and, below $g/\lambda = 2.0$, the majority of light is predominantly diffracted into the -1st with a maximum efficiency for unpolarized light of about 90% (Bragg resonance), whereas the efficiency in the +1st order has dropped below 10%.

In the Bragg regime only one or two diffraction orders are present. By choosing a proper angle of incidence, e. g., the efficiency of either TE- or TM-polarized light in one single diffraction order can attain nearly 100%, independent of the profile shape, if the Bragg-resonance condition is fulfilled [51, 52]. In this Bragg regime, Fresnel reflections have almost vanished completely.

If the period of the surface-relief structure is further reduced and becomes much smaller than the optical wavelength, we find that only the zeroth order is allowed to propagate and all the other diffraction orders are evanes-

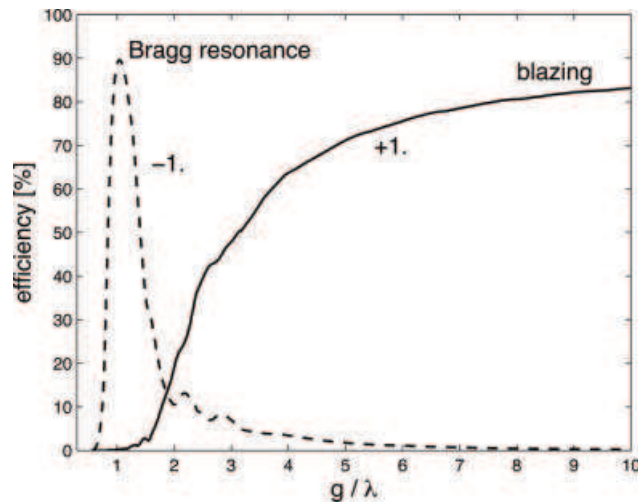


Figure 4 Diffraction efficiencies in the +1st and -1st order for a blazed triangular profile as in Fig. 2a in SiO₂ with height $h = 1.3 \mu\text{m}$ under 15° angle of incidence and $\lambda = 532 \text{ nm}$.

cent.

$$g \ll \lambda \rightarrow m = 0. \quad (7)$$

In this case, the structure behaves like an effective optical medium [53], i. e. a medium having an effective refractive index (Fig. 3). Effective media have the ability to control the effective index of refraction n_{eff} by simply adjusting the fill factor in such a way that, in principal, any value of $n_1 < n_{eff} < n_2$ is possible.

Here, the optical behavior due to the gradual transition of light through the interface depends strongly on the specific profile geometry. And different structures result in different AR properties. Such a smooth transition between two adjacent optical media and an example of the corresponding structured surface is depicted in Fig. 2b. The origin of suppression of specular reflection lies in the diffraction of optical waves when passing through a microstructured surface.

The dependence of the reduction of specular reflection on the specific profile shape can be utilized for the design of structures showing optimal performance for the desired spectral range of the specific application [54]. The scale of moth-eye features is often only just below the wavelength of incident light. Here the height, shape, and interpillar spacing period of the structures can have a pronounced effect on optical properties and must be considered for specific applications.

Considering a 1D periodic structure with a gradual index profile, the effective refractive index n_{eff} of the whole interface region is polarization dependent and can be expanded in power a series according to [55]:

$$n_{eff} = n^{(0)} + n^{(2)}(g/\lambda)^2 + n^{(4)}(g/\lambda)^4 + \dots \quad (8)$$

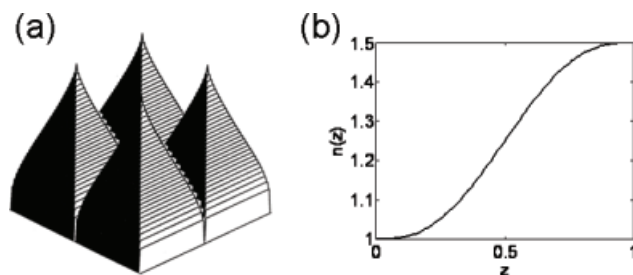


Figure 5 (a) Ideal Klopfenstein structures leading to a very smooth optical transition. (b) Corresponding transition of the refractive index n .

For each state of polarization one obtains up to the 2nd order [53]:

$$n_{\text{TE}} = \sqrt{fn^2 + (1-f)n_0^2} \quad (9)$$

$$\cdot \sqrt{1 + \frac{\pi^2}{3} (fn^2 + (1-f)n_0^2) \left(\frac{f(1-f)g}{\lambda}\right)^2 \left(\frac{n^2 - n_0^2}{fn^2 + (1-f)n_0^2}\right)^2},$$

$$n_{\text{TM}} = \sqrt{\frac{n^2 n_0^2}{fn^2 + (1-f)n^2}} \quad (10)$$

$$\cdot \sqrt{1 + \frac{\pi^2}{3} (fn^2 + (1-f)n_0^2) \left(\frac{f(1-f)g}{\lambda}\right)^2 \left(\frac{n^2 - n_0^2}{fn_0^2 + (1-f)n^2}\right)^2}.$$

Here, $n^{(0)}$ represents the effective index in the long-wavelength limit. $n^{(2)}$ and $n^{(4)}$ are dimensionless coefficients depending on the structural geometry. g/λ denotes the period-to-wavelength ratio between the grating period of the 1D profile and the respective wavelength. While closed-form expressions like Eq. (2) are feasible up to the fourth order, an exact expression of n_{eff} for 2D periodic structures, like the moth eye, has not been achieved.

To achieve an extremely low reflectance, very exceptional profile structures (Fig. 5a) known as the ‘Klopfenstein structures’ are required [56, 57]. The dependence of the refractive index obeys a quintic function on the normalized optical thickness u along the direction z at the interface

$$n = n_2 - (n_2 - n_1)(10u^3 - 15u^4 + 6u^5). \quad (11)$$

The narrow peaks and the particular vertical evolution of this special structure result in a very smooth transition at the optical interface (Fig. 5b) where the derivative at each refractive-index boundary vanishes.

Theoretically predicted antireflection structures with an optimal performance are often ideal geometrical shapes that possess sharp corners, such as the examples in Fig. 5 or Fig. 6a. Modern lithography methods, like interference lithography or laser-beam writing in combination with the etching process, are unable to realize such singular structure parts and, inevitably, result in deviations from this ideal structural shape (Figs. 6b and c) leading to corner rounding, for example. Therefore, in modeling antireflection structures, four simple profile shapes are commonly distinguished starting from the sharp-edged conical shape,

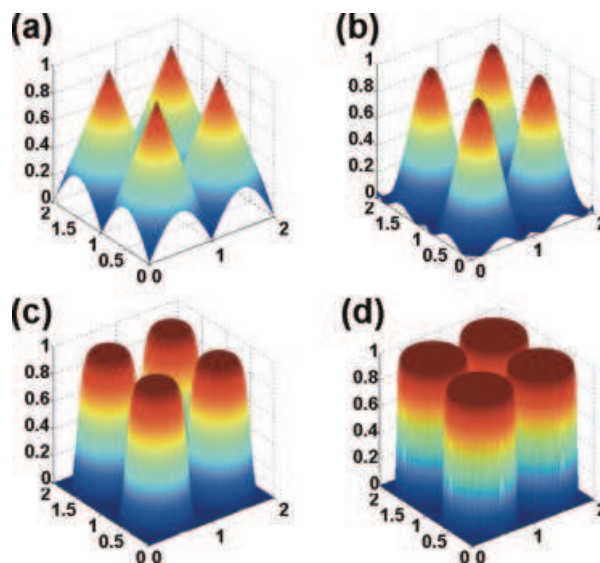


Figure 6 (online color at: www.lpr-journal.org) Four different two-dimensional profile shapes: (a) cones, (b) sinusoidal cones, (c) super-Gaussian cones and (d) cylindrical profile structures.

the sinusoidal cone shape with rounded top and the super-Gaussian profile and the cylindrical profile, where the last two structures have pronounced flat tops (Figs. 6c and d).

In particular, the super-Gaussian profile shape has been shown to accurately model sinusoidal surface relief structures that have been realized by interference lithography [52]. The profile shape is given by

$$y(x) = h \cdot \exp\left(-\left|\frac{2x - g^n}{\sigma \cdot g} \cdot \ln 2\right|\right), \quad (12)$$

where σ is the width of the profile and the exponent n is a parameter that models its flatness. In Fig. 7 the reflection behavior of a super-Gaussian profile has been compared to an ideal conical profile. The AR performance of an ideal conical profile with a sharp tip is reached for a critical height $h = 230$ nm. Increasing the height beyond this point improves the AR performance only marginally. The reflectivity remains below 0.3%. There is a weak polarization dependence. However, for super-Gaussian profiles with increasing flat-top shapes, there exists a first optimal height, which is smaller than for the conical profile and for which reflectivity is low, but the reflectivity increases and oscillates with increasing height, and it increases with the flatness of the super-Gaussian top with increasing exponent n . The optimal heights differ for the two states of polarization, so that the TM polarization requires about 10 nm deeper profile depth. The oscillation behavior with increasing height resembles the behavior of an AR coating, because the flat top induces an interference effect similar to the coating layer.

Besides the actual structure’s profile shape, the period and the height of the AR structure are two essential design parameters. For a UV-laser wavelength of 325 nm, e. g., the structure period has to be equal to or smaller than approximately 150 nm. For values below this critical period, the specular light reflection is almost independent of the struc-

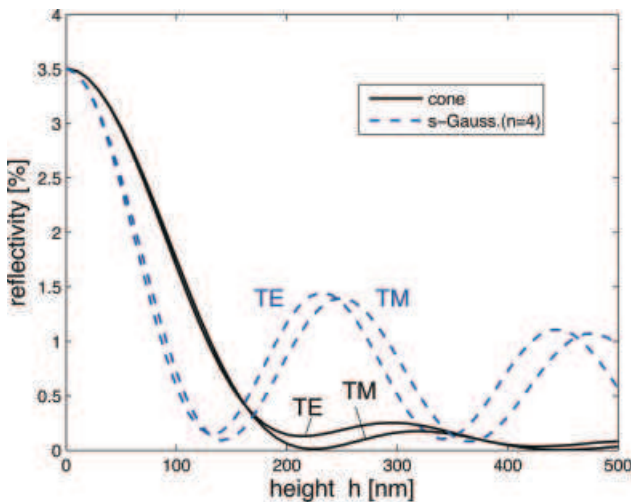


Figure 7 (online color at: www.lpr-journal.org) Reflectivity as a function of the structure height for a conical (black solid curve) and a super-Gaussian with $n = 4$ and $\sigma = 0.5$ (blue dashed curve), for both TE and TM polarization.

ture period. However, owing to manufacturing feasibility, a larger grating period is often more advantageous but may lead to unwanted light in higher diffraction orders other than the zeroth order. So, the amount of acceptable light reflection and stray light in transmission has to meet the application requirements of each specific optical system.

The second design parameter is the structure height. With increasing structure height, the smoothness of transition increases and the amount of reflected light is further reduced. The smallest acceptable structure height thus strongly depends on the choice of profile geometry. For the longer wavelength range, the depth must be larger than for the shorter range, and larger for oblique incidence (e. g., at 45°) than for normal incidence (0°).

With the proper choice of structure parameters the unique characteristics of AR structures and performance advantages over conventional multilayered AR coatings are readily seen in Fig. 8. With microstructured AR surfaces the specular reflection of light can be reduced both over a broad wavelength range (Fig. 8a) and over a broad range of incidence angles (Fig. 8b, here in the range of almost 80°).

In Fig. 8b the angular dependence of the antireflection performance is displayed (solid lines) and compared to the Fresnel efficiency (dashed lines) for three states of polarization: TE-, TM-polarized and unpolarized light. In the

interval approximately between $\pm 45^\circ$, the Fresnel reflections can be suppressed below 0.5%, nearly independent of the polarization of light (Fig. 8b). Moreover, the AR structure strongly suppresses the characteristic Brewster-type behavior at the optical interface.

2.2. Influence of local structure variations

An ideal subwavelength grating exhibits a perfect periodicity of a basic unit cell. In contrast, the homogeneity in structure period and height of real samples depends on the manufacturing process. Thus, individual protuberances of the subwavelength structure may deviate slightly from each other. The appearance of such local imperfections is related to additional spatial frequencies in the frequency spectrum of the grating. If these additional frequencies are related to periods for which the zero-order condition is no longer fulfilled, higher propagating diffraction orders are introduced and the zeroth-order efficiency is decreased. In particular, periods that are slightly larger than the limiting period of the zero-order condition will induce a deflection in large spatial angles. On the other hand, very large periods are also associated with diffraction orders in small angles.

To simulate the influence of the imperfectness of the subwavelength grating on the transmittance of an AR structure, both a statistical height variation and also statistical variation of the lateral spacing between single protuberances was investigated by rigorous numerical methods [58].

Figure 9 shows the mathematical approach schematically. Starting with perfect periodic Gaussian-shaped protuberances (on the left), a statistical height variation was introduced (on the right, upper part) and a variation of the lateral spacing between single protuberances (on the right, lower part) was assumed. Both the height variation and the local displacement between the protuberances were assumed to follow a statistical Gaussian distribution. The three illustrations of Fig. 9 show only 4 individual protuberances for simplicity, but the calculations were in fact carried out with 128 protuberances, which offer a sufficient convergence of the simulations. Under these conditions the resulting data does not change more than 0.1%.

The calculated results for the sum of zero-order reflected and transmitted light as a function of the wavelength for both cases are displayed in Fig. 10. In the subfigures, each data curve corresponds to different standard deviations. The mean structure height was assumed to be 235 nm, which cor-

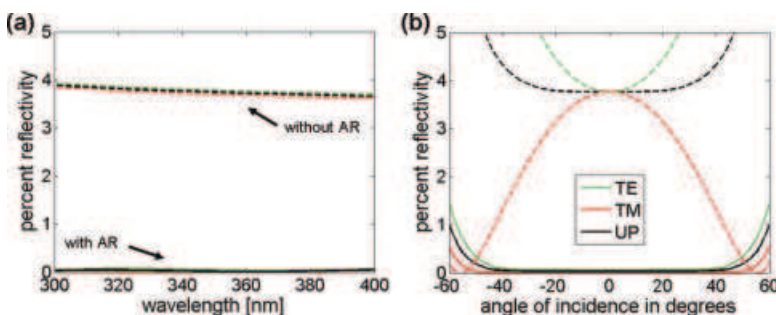


Figure 8 (online color at: www.lpr-journal.org) Efficiency performance in reflection of AR structure as in Fig 5a for the zeroth-order light with (solid) and without (dashed) AR structures: period of 150 nm with a structure height of 440 nm. (a) Dependent on the wavelength for normal incidence and (b) dependent on the angle of incidence for TE- and TM-polarized and unpolarized light (UP).

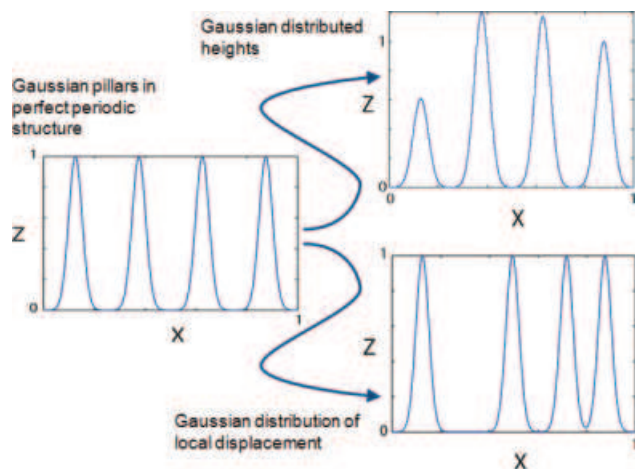


Figure 9 (online color at: www.lpr-journal.org) Theoretical approach to simulate a more realistic profile model. Instead of a perfect periodic structure (left), a height variation (top right) or a statistical distribution of the center position of the individual protuberances (bottom right) is assumed.

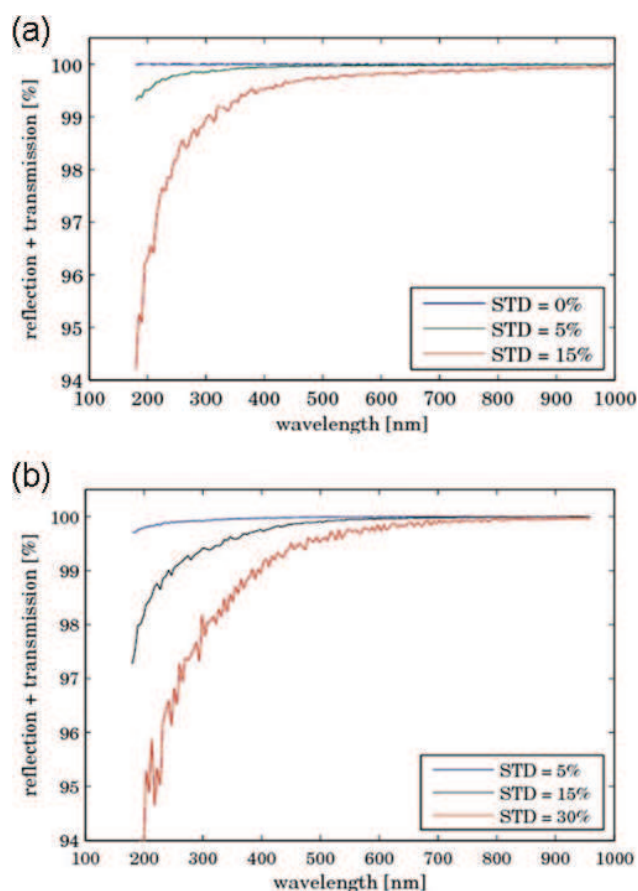


Figure 10 (online color at: www.lpr-journal.org) Total efficiency in transmission and reflection, if the profile is statistically varied with defined standard deviations (STD) according to the configurations in Fig. 7 for (a) the variation of height and (b) for the variation of the grating pitch.

relates to a reflectance minimum at 325 nm. The Gaussian-shaped protuberances had a mean distance of 80 nm for these simulations. Both cases demonstrate a strong increase of the scattering effects with increasing standard deviation and decreasing wavelength. From these results, it follows that a strong anti-reflective behavior in the UV or even deep-UV can only be guaranteed if irregularities of either kind, which lead to spatial frequencies violating the zero-order condition, are avoided.

3. Manufacturing technologies: top-down approach

In this context, top-down approach means to transfer a lithographical technique, which is already established for the manufacturing of large-scale structures, to the subwavelength range.

Generally in top-down technologies, it is suitable to distinguish between serial and parallel processes. As a serial technique direct e-beam writing offers the necessary high lateral resolution for subwavelength structures and already has been applied successfully to manufacture such effective media [30, 59, 60]. However, the main disadvantage of serial direct writing techniques is often the exceptionally long time consumption in the fabrication of subwavelength structures over a relatively large extended area (as compared to the structure period).

On the contrary, parallel processes offer the advantage of a structuring in a single exposure step. For example, mask-based contact lithography allows the structuring of subwavelength features [61] but, unfortunately, this technique is susceptible to contamination and also limited to plane substrates. An advantageous alternative parallel process is interference lithography (IL), which is fast, contact free and also applicable at least to weakly curved substrates such as concave or convex lenses. So, it can be exploited for various structuring configurations, as will be discussed in the following paragraphs.

Interference lithography is a historic technique that was introduced to manufacture spectroscopic gratings already in the 19th century [62]. Since the introduction of short-wavelength and high-power lasers in the early 1970s IL became a very popular manufacturing technology for spectroscopic gratings [63, 64] with the potential to tailor efficiency- and polarization-optimized grating profiles [65] and also to fabricate imaging diffractive elements, e. g., for microspectrometers [66]. The basic process step in the IL technique is the exposure of a photoresist-coated substrate with an interference fringe pattern generated by coherent beams. Figure 11 shows the schematic of a typical IL exposure setup. A laser beam is separated into two light paths, which are then directed with mirrors, spatially filtered, expanded and collimated. In the intersection area an interference fringe pattern is generated, which exposes a linear grating in the resist on the substrate. During the recording process, a latent structure is captured in the resist, which is transformed into a continuous surface profile in the subsequent development process. After the development process the structure may

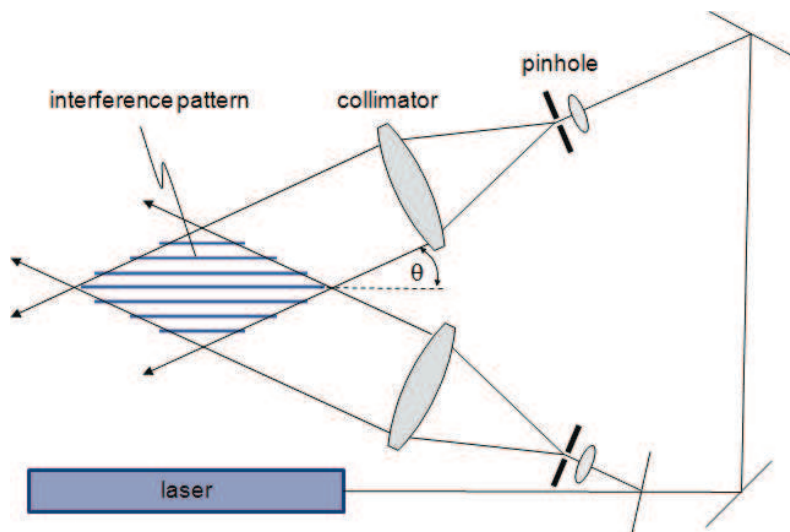


Figure 11 (online color at: www.lpr-journal.org) Schematic drawing of an optical exposure setup used for interference lithography. Laser light is split into two beams that are spatially filtered, collimated and redirected. In the overlap area an interference pattern is generated that is used for the recording of the periodic structure.

either be used directly or, after a stabilization of the pattern structure, an adjustment of the profile depth can be realized by selective reactive ion beam etching.

In interference lithography, the grating period depends on the exposure wavelength, the refractive index of the ambient material and the angle between the interfering light waves. Under normal ambient conditions (air), the minimal obtainable grating period is of the order of half of the exposure wavelength. Especially with the employment of short-wavelength lasers, IL becomes a very appropriate basic technology also for the fabrication of anti-reflective moth-eye structures [67–69].

With the interference of two plane waves only one-dimensional periodic intensity profiles can be generated, which results in a linear grating type. To manufacture a two-dimensional periodic moth-eye structure, double-exposure techniques are necessary with a defined rotation of the substrate between the subsequent exposure steps. By two exposures and an intermediate rotation of the sample holder by 60° or 90° , hexagonal and two-dimensional (2D) crossed gratings can be manufactured.

Figure 12 shows the SEM picture of a 2D hexagonal structured moth-eye array generated by double-exposure IL made by the company Holotools [38]. The perfect periodic structure possesses a pitch of 300 nm and an average depth of 350 nm. When structured in a polymer, the surface reflectivity decreases typically to 0.6% over a broad bandwidth from 400 nm to 700 nm. A holographic polymer structure is also suitable to serve as the basic tool for further processing to replication moulds needed for imprint technology, injection molding or thermal embossing.

Immersion configurations are used in the IL process to further reduce the feature size. This means that an optical high-index material is introduced in the direct environment of the substrate to be exposed. In the accompanying exposure setup the photoresist-coated substrate is typically sandwiched between UV-transparent prisms using an immersion liquid with a matched refractive index. The minimal period is decreased by a factor given by the refractive index of the immersion medium.

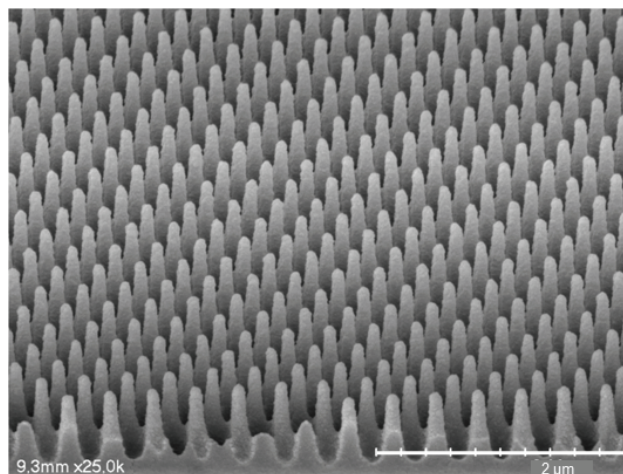


Figure 12 Scanning electron microscope image of an artificial ‘moth-eye’ surface generated by Interference Lithography (courtesy of Volkmar Boerner; Holotools, Freiburg).

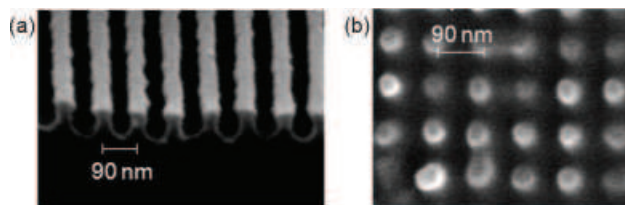


Figure 13 Scanning electron microscope images of ‘moth-eye’ structures with periods < 100 nm (10 800 l/mm). The gratings were obtained by single- (a) and double- (b) exposure techniques using 266-nm immersion lithography.

The scanning electron microscope images presented in Fig. 13 display patterns with a grating period of nearly 90 nm (10 800 l/mm) that were obtained by single- (left) or double-exposure (right) using 266 nm (frequency-quadrupled Nd-YAG laser) immersion lithography. These structures are developed to serve as AR coatings for deep-UV applica-

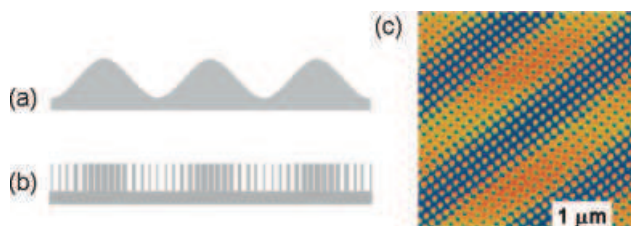


Figure 14 (online color at: www.lpr-journal.org) Schematic illustration of a sinusoidal surface relief profile (a) and a subwavelength structured analog (b). In (c) the topography of a modulated subwavelength grating is shown that was manufactured by a triple exposure IL process (AFM measurement).

tions [16]. For that purpose the polymer profile has to be transferred into the fused-silica substrate by the reactive ion etching process.

Interference lithography is also applicable to manufacture diffractive optical elements as modulated subwavelength gratings. The basic idea of such diffractive structures is that each individual period of the diffractive element, which is larger than the working wavelength, is composed of a sublattice with variable width of lines and spaces, forming a subwavelength surface profile. Controlling the feature size of the subwavelength structures allows a lateral tailoring of the local effective index of refraction.

The principal concept is illustrated in Fig. 14. A classical sinusoidal profile guarantees a continuous phase shift along each individual period by varying the depth of the structure in a material of constant refractive index (Fig. 14a). In a modulated subwavelength grating (Fig. 14b), the sinusoidal gradient material is approximated by the variation of the structure dimensions of binary subwavelength features. Such structures, especially in the form of blazed binary gratings, allow a high-efficient coupling of light into the first diffraction order [28], which have been shown to exceed the properties of a conventional blazed grating [30], if the subwavelength structure causes a pillar-waveguiding effect that is responsible for a drastic reduction of the shadowing zone [70]. Based on this principle Wollaston prism-like devices are also manufactured and investigated [53] and sinusoidal transmittance subwavelength metallic structures for application in the midinfrared wavelength range are realized [71].

Figure 14c shows the topography measured by AFM of a modulated subwavelength grating manufactured by a triple-exposure IL process. Here, in the initial first two steps the two-dimensional subwavelength structure is exposed to yield a period of 200 nm. The directly following third exposure step, with a period of 2 μm , superimposes the initial grating so that finally, after the development process, the subwavelength modulated sinusoidal topography is created.

As mentioned above, another very important property of the IL is to generate moth-eye structures on curved surfaces that are either concave or convex, or even aspheric or free-formed. However, difficulties occur when the radius of curvature of the target substrate is too small.

This limitation becomes obvious in Fig. 15, which displays schematically the basic exposure setup for plane sub-

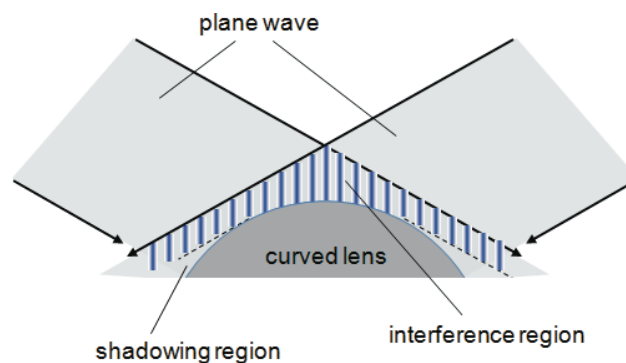


Figure 15 (online color at: www.lpr-journal.org) Illustration of the geometrical conditions when using plane-wave interference lithography to structure curved lenses. The central region is readily accessible, in the boundary area shadowing effects occur.

strates but now is applied for curved lenses. For the sake of simplicity, the schematic neglects refraction and also multiple reflection effects at the lens surface. At the apex of the lens the exposure conditions are similar to the situation when structuring plane substrates. Here, the plane waves overlap undisturbed and allow the exposure of the photoresist with a high interference contrast. Near the edge of the lens, shadowing effects are introduced and restrict the maximum curvature of the substrates.

In a more detailed consideration, also taking into account the wave propagation inside the covering resist and the lens material, it could be shown that there is still an interference pattern in the geometrical shadowing region but with significantly reduced contrast, so that a proper exposure over the whole surface is not guaranteed. In principle, with a modification of the inclination angle between the plane waves, it is possible to decrease the accessible radius of curvature of the lens, but this modification will simultaneously increase the periodicity of the structure so that the anti-reflective behavior is shifted to longer wavelengths.

4. Manufacturing technologies: bottom-up approach

Antireflective surfaces have been fabricated by bottom-up methods such as deposition of multilayered or porous films directly on the surfaces of optical devices for a long time. Porous films can resemble effective media that are characterized by a gradually changing refractive index leading to highly anti-reflective surfaces. Mainly sol-gel techniques have been used that rely on hydrolysis and condensation reactions of metal alkoxides leading to the formation of a sol [72]. This sol is applied on a substrate and crosslinked thermally or by irradiation [73–75]. The porosity of the resulting coatings and, consequently, their refractive index can be controlled by incorporation of colloids that are removed upon thermal treatment [76] or by addition of heterometal alkoxides [77]. Antireflective coatings based on microcrystalline alumina, which have been prepared using a sol-gel process, are already applied to camera lenses and distributed

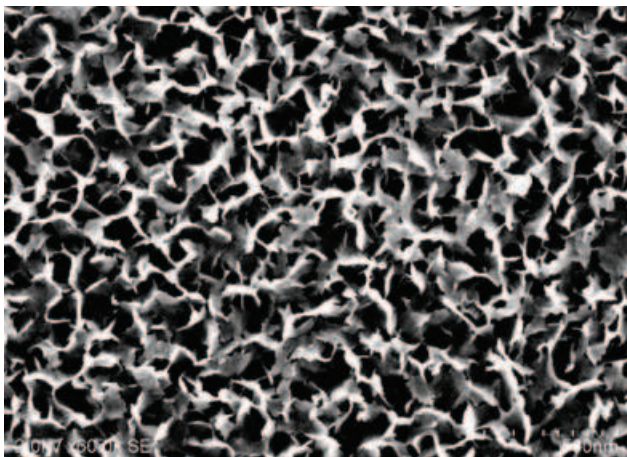


Figure 16 FE-SEM image of an Al_2O_3 film immersed in hot water. A microcrystalline alumina film with a patterned nanostructure is formed which shows anti-reflective behavior. (Courtesy of Takeharu Okuno, Canon, Japan.)

by Canon [78]. A representative SEM image of the nanostructured surface is shown in Fig. 16. The reflectance of these coatings is not only lower in absolute terms but also exhibits better wavelength and angle-of-incidence independence in comparison to antireflection coatings composed of multilayers. A more detailed discussion of this application example is found in Sect. 5. However, anti-reflective coatings prepared by sol-gel techniques are composed of stochastic subwavelength structures that should have lower transmission efficiency especially in the UV range in comparison to periodic subwavelength structures due to local variations in the nanostructure (height and local displacement) leading to light scattering (see Sect. 2.2).

The fabrication of biomimetic anti-reflective surfaces resembling periodic subwavelength structures on moth's

eyes is still a challenge due to the mainly employed time consuming and expensive top-down techniques. Hence, fast and low-priced bottom-up methods are highly desirable in the process of generating anti-reflective surfaces on areas large enough in order to be interesting for optical applications. Figure 17 gives an overview of fabrication methods for biomimetic anti-reflective surfaces consisting of pillar-related subwavelength structures that are based on bottom-up techniques.

The first attempts to implement a bottom-up technique in the fabrication of periodic subwavelength structures for anti-reflective applications were targeted on the replacement of the etching masks that have previously been fabricated by e-beam or photolithography and transferred into the substrate by reactive ion etching leading to the desired nanostructured surface. The most commonly used bottom-up method for the preparation of etching masks is colloidal lithography. This very simple, cost- and time-efficient technique generates two-dimensional hexagonally close-packed colloidal crystals from dispersions of wet-chemically synthesized silica or polymer nanospheres by self-assembly. Several deposition methods can be employed, such as lift-up of a colloidal monolayer floating on an interface, dip coating, electrophoretic or template-guided deposition as well as spin coating. The dimensions of the colloidal array can easily be controlled by changing the size of the colloidal particles. Details on colloidal lithography can be found in several articles and reviews [79–82]. The colloidal array serves as a mask upon subsequent dry etching. Mainly, reactive ion etching (RIE) has been employed for the fabrication of subwavelength nanostructures [83–85]. The etching conditions such as pressure, chosen gas composition, temperature, etching time, etc., determine the morphology of the resulting nanostructure and its height [86,87]. In addition, the etching mask material has an influence on the etching result as the etch rates of mask and substrate differ. Depending on the

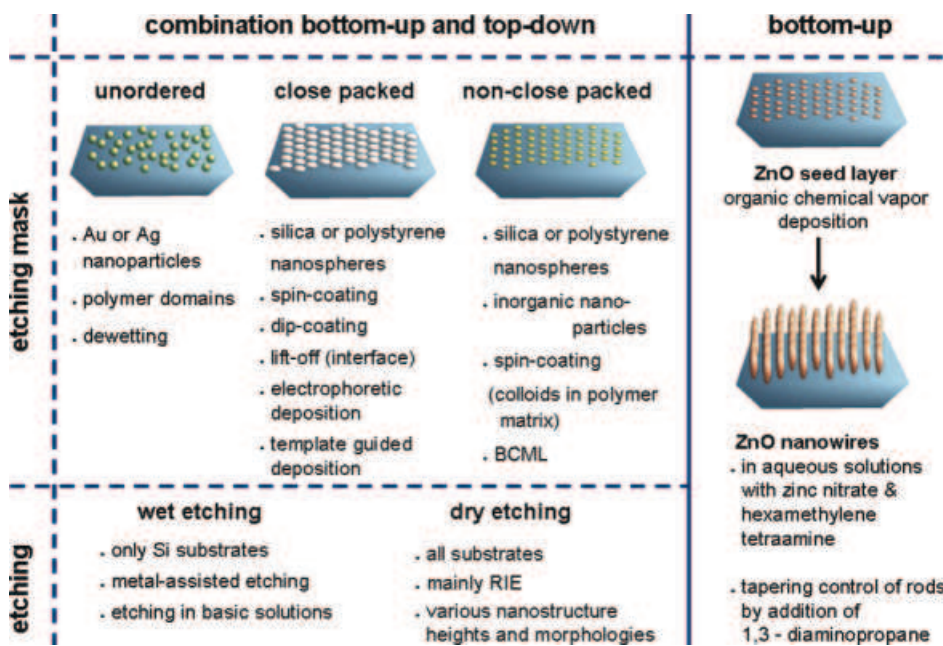


Figure 17 (online color at: www.lpr-journal.org) Summary of fabrication methods for biomimetic anti-reflective surfaces based on bottom-up techniques.

used mask material the size of the etching mask (colloids) is also gradually reduced upon etching and mostly faster than the underlying substrate material, enabling the fabrication of cone-shaped structures.

Conventional colloidal lithography is limited to the fabrication of close-packed arrays, whereas moth-eye anti-reflective structures with subwavelength protrusions possess nonclose-packed characteristics (nonclose packed refers to gaps between colloids and NOT to packing of spheres) [88]. If reactive ion etching is used to generate anti-reflective nanostructures the utilization of close-packed or nonclose-packed etching masks can lead to the same etching results as the close-packed mask can easily be transferred into a nonclose-packed mask by a prior plasma treatment [80]. However, this additional etching step could be avoided by the fabrication of nonclose-packed colloidal structures. Jiang et al. developed an appropriate technique that is based on shear-aligning concentrated colloidal suspensions using standard spin-coating equipment and enabling the production of wafer-scale, nonclose-packed colloidal crystals [89]. These two-dimensional arrays have been used for the fabrication of anti-reflective surfaces on inorganic materials using RIE or as templates for the preparation of polymer-based anti-reflective coatings [90–92].

Despite the enormous progress in the field of colloidal lithography, it is still difficult to produce well-ordered pattern with lateral distances below 100 nm, which are required for optical applications in the UV range. An adequate bottom-up method to achieve such a high resolution is block-copolymer micelle nanolithography (BCML) and has been applied to the fabrication of anti-reflective surfaces by Spatz et al. [93, 94]. Here, nanoparticle arrays were prepared by BCML that serves as a mask upon subsequent RIE (Fig. 18). In BCML, polymers are used that consist of different blocks with different solubility in a selective solvent. The simplest class of such an amphiphilic copolymer is an AB diblock-copolymer composed of a hydrophilic and a hydrophobic block. Upon dissolution in a hydrophobic solvent the block-copolymer can self-assemble into micelles with a hydrophobic shell and a hydrophilic core that can be loaded with a metal salt. If a substrate is immersed in this solution and slowly retracted, a monolayer of quasi-hexagonally ordered loaded micelles is formed upon solvent evaporation. The intermicellar distance can be controlled by the block-copolymer itself, the polymer concentration and the retraction speed. Figure 19 displays SEM images of gold nanoparticle arrays prepared using diblock-copolymers with different block lengths leading to a variation in interparticle distances. To finally create a nanoparticle array on the substrate, the polymer matrix is removed and the metal salt reduced to metal nanoparticles by plasma treatment. BCML can be applied to a huge variety of substrates and additionally allows for the fabrication of different semiconductor and metal nanoparticles that possess different etching contrasts [95, 96]. In addition, the size of the metal nanoparticles and consequently of the etching mask can easily be controlled by a chemical reaction called electroless deposition [93]. For the fabrication of anti-reflective surfaces, gold nanoparticles acted as a mask upon subsequent RIE

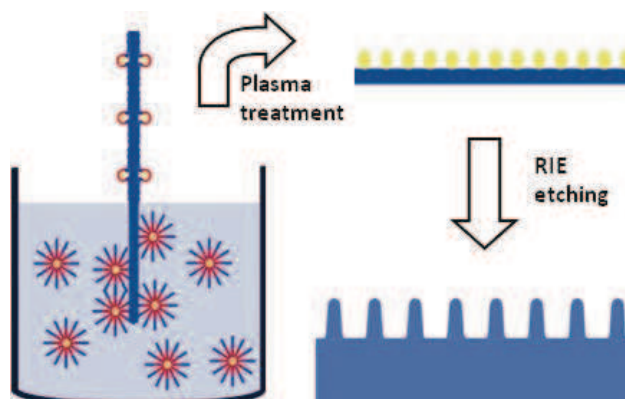


Figure 18 (online color at: www.lpr-journal.org) Schematic illustration of the fabrication method for anti-reflective surfaces based on BCML and RIE. Diblock-copolymers can form spontaneously micelles with a hydrophilic core and a hydrophobic shell in solution. Metal salts can be loaded into the micellar core and the resulting loaded micelles are deposited on the substrate surface by either spin coating or dip coating. By choosing the appropriate deposition parameters a monolayer of quasi-hexagonally close-packed micelles self-assemble on the substrate surface. Plasma treatment removes the polymer and reduces the loaded metal salt, leading to the formation of a metal nanoparticle array. This array serves as a mask upon subsequent RIE, allowing the fabrication of anti-reflective surfaces.

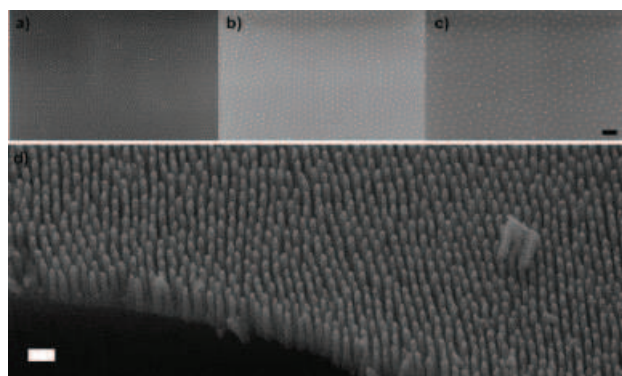


Figure 19 SEM images of gold nanoparticle arrays fabricated by BCML and a nanostructured anti-reflective surface generated by RIE using gold nanoparticles as etching mask. BCML allows for an easy control of the interparticle distance by choosing the appropriate parameters. The center-to-center distance between the nanoparticles is: a) approximately 40 nm, b) approximately 72 nm, and c) 99 nm. d) Antireflective surface etched into fused silica. Scale bar: 200 nm.

processing. The lateral gold nanoparticle pattern periodicity determines the spacing of the etched nanostructure and the etching parameters determine their morphology and height. Using this method, surfaces with tailored anti-reflective properties can easily be fabricated that show optimum performance for specific applications. These structures not only show broadband anti-reflective behavior covering the wavelength range from deep ultraviolet to visible light but can

also provide nanostructured surfaces optimized for excimer-laser applications. The transmission of light was improved by a factor of 5% for 193 nm and 3% for 248 nm.

In particular, for the fabrication of anti-reflective nanostructures on silicon other techniques have been developed. Often unordered etching masks were used composed of either metal nanostructures (metal nanoparticles or metal nanoislands formed by dewetting) [97, 98] or domain structures generated by Langmuir–Blodgett techniques from mixtures of stearic acid and poly-(ethylenimine) on water surfaces [99]. Moreover, chemical etching can be employed for the preparation of biomimetic subwavelength structures on Si. Basic solutions (KOH) in combination with hydrofluoric acid (HF) and metal nanostructures – so-called metal-assisted etching – can etch the desired nanostructure into silicon substrates [100].

Fabrication methods of biomimetic anti-reflective surfaces solely based on bottom-up methods are still rare. Recently, Lee et al. [101] synthesized biomimetic anti-reflective ZnO coatings on silicon substrates using a two-step seeding and growth method. Textured ZnO nanorod arrays were wet-chemically prepared via low-temperature aqueous solution deposition. Depending on the solution growth conditions, the morphology and especially the shape of the ZnO nanorod tips could be controlled leading to the desired gradually refractive index profile that can lower the global weighted reflectance to 6.6%. A combination of a fused ZnO layer at the bottom and a nanorod array with tapered tips led to broadband anti-reflective behavior. However, the rigidity of these structures hampers their application in the area of flexible photovoltaic modules. In 2010, Kim et al. [102] solved this problem by infiltration of PDMS into the ZnO nanowire array.

Which of the two manufacturing technologies, the top-down or the bottom-up approach, is more advantageous over the other, particularly for optical applications, depends on the function and properties of a specific optical element. First, the wavelength range in which the AR structure is supposed to work is limited by the period of the AR structure and the depth attained by the subsequent etching technique. The structure depth determines the long-wavelength end and the homogeneity determines the short-wavelength range, as also discussed in more detail in Sect. 2.2.

For large dimensions, the bottom-up approach, since it is based on a self-organization process, is known to build spontaneous structure domains, in which, e. g., hexagonal and stripe-shape patterns coexist. So the AR performance may vary locally over the element.

Finally, the form of the surface to be AR structured puts a challenge to the manufacturing process. While plane substrates are easily spin coated for interference lithography, AR structures on convex and concave substrates may be limited by their radius of curvature for top-down approaches. This becomes even more critical for both micro-optical elements, such as microlens arrays, and microstructured gratings, such as the blazed gratings. So, the bottom-up approach is the preferred choice of technology for these types of optical elements.

5. Applications of moth-eye structures in optics

5.1. For high-end imaging lenses

The development of high-end imaging photolenses is permanently driven by the demand to increase the performance of the system in terms of image quality, faster lenses with wider zoom ranges, and, simultaneously, to reduce weight and volume of the lens system. To meet these demands, modern lenses make frequent use of, e. g., ultralow dispersion glass, aspherical lens elements and lenses with large curvatures. Unfortunately, a large lens curvature tends to generate strong reflections, which may be the source of flaring, ghosting and other harmful or unwanted light. Especially when using digital camera CCD and CMOS imaging sensors, which have a higher reflectance than conventional films, this problem becomes crucial by causing the so-called digital ghosting.

To meet these requirements, high-performance anti-reflective coatings have to be developed. Unfortunately, classical multilayer coatings are inadequate to perform a high anti-reflective function over the entire visible bandwidth and, simultaneously, across a wide range of incidence angles, e. g., from 0 to 45 degrees.

To overcome this problem, the Japanese scientist Takeharu Okuno from the company Canon presented a solution based on a subwavelength-structured coating, which was applied to Canon's sophisticated EF $f/1.4$ L II USM lens system [78].

Figure 20 shows schematically the cross section of the lens design of the EF $f/1.4$ L II USM lens optics. Due to design simulations, which indicated that reflections on the inner surface of the first element (dashed line) have an enormous influence on the image quality, this surface was coated with a subwavelength anti-reflective structure.

Because, first, the glass of the first lens element has a rather high refractive index ($n_d = 1.84$) and, on the other hand, the maximum (bulk) refractive index of the coating material is limited to a value of 1.40, a simple application

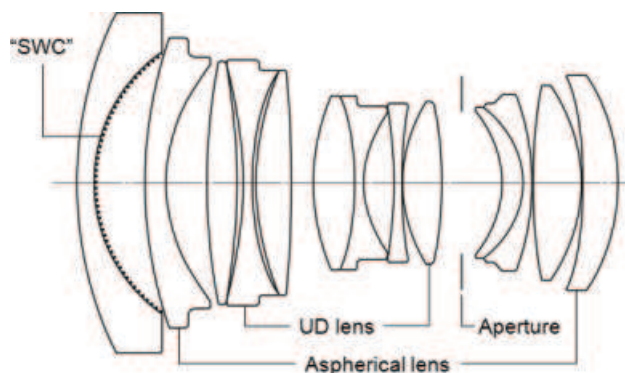


Figure 20 Cross-sectional view of Canon's sophisticated EF $f/1.4$ L II USM lens system [72]. The inner surface of the first element (dashed line) is equipped with a subwavelength structured AR coating (courtesy of Takeharu Okuno, Canon, Japan).

of the subwavelength structure on top of the substrate is not sufficient for a high anti-reflective performance.

A solution was found by inserting an intermediate layer between the first lens element and the subwavelength structure. With this solution the subwavelength structure cancels reflections arising from the refractive index transition from 1.0 to 1.4, and the intermediate layer acts as a single-layer anti-reflective coating, which reduces reflections arising from the refractive-index transition from 1.40 to 1.84.

For the coating of the intermediate layer a sol-gel process with silica (SiO_2) and titanium oxide (TiO_2) was applied. By varying the ratio of both ingredients in the solution, the refractive index of the layer is adjustable over a certain range. This characteristic offers the advantage to match the refractive index of the intermediate layer to the refractive index of different lens substrates.

As a consequence, the reflectance properties of this final subwavelength coating are not only beneficial in absolute terms but they exhibit a much better wavelength spectrum and highlight an outstanding angle-of-incidence independency.

5.2. For micro-optical elements

In mosquito eyes, for example, nature combines micro- and nanostructures to form hierarchical arrays. To transfer these ideas to our technical world, different approaches have been made. One of the most direct alternatives involves the replication of the hierarchical structures from biotemplates found on cicada eyes [103]. Xu et al. [104] followed the bioinspired mosquito eye by combining self-assembled polymer spheres and nanoimprint lithography. With this approach it was possible to create nanopillars on microscale round protrusion arrays. These hierarchical structures provide a multifunctional light-escaping architecture that allows, for example, to increase the light output power of light-emitting diodes [105].

Microstructured optical surfaces, such as diffractive elements or refractive microlens arrays, experience a strong increase in the demand for diverse applications, especially, in sophisticated spectroscopic instruments or in laser-based illumination systems for beam shaping and coherence management. Due to the complex geometric features of such micro-optical elements and also from the optical performance demands, the AR coating of such elements is quite challenging. Recently, it was found that the concept of moth-eye structures can also be transferred to micro-optical elements, which is also accompanied by some specific difficulties. In particular, when using photolithographic processes, the resist coating on the pre-microstructured surface will lead to a completely inhomogeneous resist layer thickness. To overcome this effect, Disch et al. [106] applied a negative-tone photo resist in a back-surface exposure setup and demonstrated the capabilities on a microstructured Fresnel lens. It has also been shown that the BCML structuring technique is an appropriate method to transfer the ‘moth-eye’ structure to diffractive binary gratings.

Figure 21 depicts the topography of two binary grat-

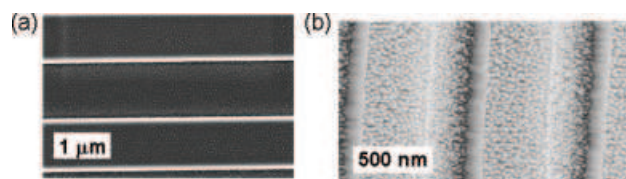


Figure 21 Scanning electron microscope images of binary gratings equipped with subwavelength structures. (a) binary grating covered with gold nanoparticles before edging. (b) Final AR subwavelength structure transferred into a binary diffractive grating.

ings equipped with subwavelength structures measured by scanning electron microscopy. The structure of Fig. 21a is a binary grating covered with gold nanoparticles before etching. The bars have a height of 850 nm and the grating period is $5\ \mu\text{m}$ (original grating structured by B. Kley, Institute of Applied Physics at Friedrich-Schiller-University, Germany). In the dip-coating process, in which the initial gold particle mask is created on top of the surface, the sample is pulled out of the solution in a direction parallel to the desired grating grooves. Although the overall subwavelength structure shows a well-regulated order, a more dense concentration of the protuberances near the edges of the lines can be observed (Fig. 21b).

The fabrication of microlens arrays that have ‘moth-eye’ structures on their surfaces was also demonstrated. Oh et al. [107] developed a thermal imprinting process to replicate microlenses in a polymer substrate that is followed by a plasma treatment to form the subwavelength anti-reflective structures.

5.3. For polymer optics

The transfer of the moth-eye principle to polymer optical elements offers some characteristics that are interesting, especially for high-volume or large-area applications. Hereby, an essential aspect concerns the possibility to generate the refractive curvature of the optical element simultaneously with the AR property in a single replication step such as in injection molding or hot embossing. This means, in the replication tool (mold) the global wavefront-forming curvature is already superposed by the subwavelength AR structure. Instead of the separated manufacturing of the lens and the AR layer system as in a classical process the combined structuring allows potentially a low-cost production.

A further advantage becomes obvious when the optical system is specified for a large temperature range. In conventional systems a strong difference in the thermal expansion coefficients between the substrate and the coating material may cause adhesion problems and layer damage.

Besides all potential benefits, there are also significant challenges concerning the mass replication of moth-eye structures in polymer substrates. For example, the subwavelength feature size is related to a large contact area between the mold and the replicated optical element, which may be accompanied by strong adhesion forces and lead to release problems during the deforming step. In consequence,

this will influence the endurance of the mold, so that its lifetime is limited or, at least, the number of possible replication steps is reduced before a refurbishment of the tool becomes necessary.

Another challenge concerns the contamination of the AR surface, especially with fingerprints. Although the subwavelength structures show an unexpected mechanical stability to cleaning procedures, a dry removal of contamination is often inefficient. For example, the fat from the fingerprints fills the grooves of the moth-eye structure or fractions of the cleaning tissue will adhere to the surface. Some adequate ways to clean the surface are made by using rinsing water, eventually with an additional drop of dish cleaner [69].

A successful application of moth-eye structures on polymer surfaces was demonstrated for the flat-panel display market by Gombert and Bläsi from the Fraunhofer Institute (ISE) [69] in cooperation with Boerner from the company Holotools [38]. On information displays, the readability of the content may be significantly reduced by reflections of the ambient light on the display screen. Even indoors the mirror images of lamps or windows on the screen are very disturbing. Due to the high luminance of the respective light sources, it becomes advantageous to combine the subwavelength AR structure with antiglare surfaces that scatter the reflected light into small angles [108].

The successful basic manufacturing process was interference lithography with multiple exposures, which allows the structuring of both the aperiodic and very smooth antiglare structure and also the subwavelength grating with a high aspect ratio. Hereby, in one exposure step, a masked diffuser was inserted in the expanded laser beam, which produces well-defined speckle patterns to generate the antiglare structure. The superposing moth-eye structure is manufactured in a way that has been described in Sect. 3.

By adjusting the process and incorporating multiple different exposures, it was possible to manufacture optimized structures with very good optical properties [109]. The result is depicted in Fig. 22 and shows the image of a flat-panel display with standard antiglare surface (left side) and combined moth-eye anti-reflective and antiglare (MARAG™) surface (right side). Meanwhile, the company MacDermid Autotype in Wantage, UK [110] sells various optical films with moth-eye structures that exploit again the basic manufacturing approach as described in Sect. 3.

An alternative approach to create subwavelength AR structures on polymer optical elements is based on a low-pressure plasma ion etching process, which creates self-organized nanostructured surfaces in polymers such as the popular PMMA (polymethylmethacrylate) or the eyeglass material CR39 (polydiethyleneglycol-bis-allyl-carbonate) [111, 112]. In fact, this process requires an independent step in addition to the global forming of the optical element, but also allows the AR functionalization of complex-formed substrates (e. g. Fresnel lenses) and does not induce further difficulties in the release process.

Typically, the self-organized stochastically arranged AR structures reveal a bump-like appearance with a depth of 200–300 nm and a distance between surface features of approximately 70–100 nm (Fig. 23a). As another desirable op-



Figure 22 (online color at: www.lpr-journal.org) Photo taken from a flat-panel display with standard antiglare surface (left side) and combined 'moth-eye' anti-reflective and antiglare surface (right side). As an object on the flat-panel display the compound eye of a moth is shown (courtesy of Volkmar Boerner; Holotools, Freiburg).

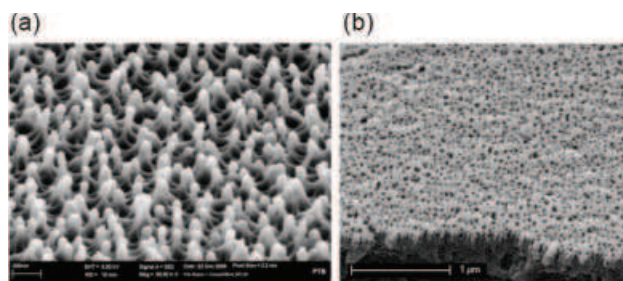


Figure 23 Scanning electron microscope images of self-organized stochastically AR structures fabricated by plasma etching. (a) Bump-like structure based on a direct plasma etching process applied to a polymer (PMMA) surface. (b) Sponge-like polymer surface realized by plasma etching with an initial assist dielectric cover layer (courtesy of Ulrike Schulz and Norbert Kaiser; Fraunhofer IOF, Jena).

tical result, these structures possess excellent antireflection behavior for light of normal and oblique incidence, simultaneously.

The generation of subwavelength, stochastically distributed anti-reflective structures by direct plasma etching was initially restricted to only a few polymers. In an advanced procedure [40], an initial dielectric top layer (TiO_2 , SiO_2) with a thickness range from 0.5 to 2.5 nm is deposited on the polymer prior to the plasma etching. Today, almost all types of polymeric materials can be equipped with anti-reflective properties. This improvement allows the generation of a broad range of different subwavelength morphologies on polymers in a shorter time, including bump- and

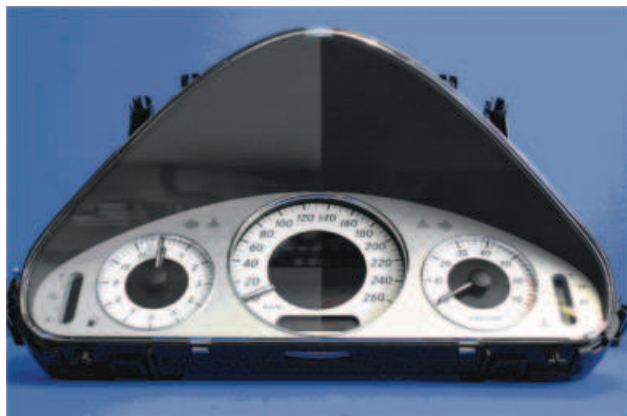


Figure 24 (online color at: www.lpr-journal.org) Instrument panel of an automobile: Left side: untreated area, and right side: AR-coated area. The inside of the AR region is treated with the plasma-etching process, the corresponding outer surface is covered by a conventional layer system (courtesy of Ulrike Schulz and Norbert Kaiser; Fraunhofer IOF, Jena).

sponge-like structures (Figs. 23a and b). The structured surfaces show a tendency to have a gradient in the filling factor from top to bottom and, therefore, also provide a graded refractive index that increases with depth.

Different theories attempt to explain the mechanism of the structure formation [40]. In a first approach it was assumed that the deposited material grows as a noncontinuous film forming islands. A second assumption is that the continuous initial layer is dispersed into pieces during the plasma treatment caused by the much higher thermal expansion of the substrate compared with that of the initial layer material. Thus, a mask formation could take place when the sample is heated by the plasma. However, both ideas could not be proven up to now.

As an application example, Fig. 24 depicts the instrument panel of an automobile, which distinguishes an anti-reflective area (right side) from an untreated area (left side). The difference in the optical behavior becomes rather obvious here. It has to be mentioned that only the inside of the AR region of the polymer glass is treated with the plasma etching process. The corresponding outer surface is covered by a layer system.

5.4. For integrated optoelectronic devices: solar cells, photodetectors, and LEDs

Optoelectronic devices such as light-emitting diodes (LEDs), photodetectors, photovoltaic or thermophotovoltaic cells are based on semiconductor materials. The high refractive indices of these materials are responsible for the very large reflectivity, so that up to 40% of the incident radiation is reflected back from the untreated surface. To increase the efficiency of the optoelectronic devices an appropriate AR coating is indispensable. Also, for these applications the classical antireflection coatings are only effective over a limited spectral range, and suffer from mechanical and

thermal instability, or adhesion problems and thermal mismatch. Therefore, the concept of the subwavelength anti-reflective structures was also investigated for applications on semiconductor-based optoelectronic devices. Hereby, most often it is not only essential to achieve the required optical and mechanical properties of the structured AR coating but also to provide an adequate technology chain, allowing a cost-sensitive production technology.

A very promising application field of subwavelength anti-reflective structures concerns photovoltaic systems that use solar cells to convert solar power to electricity. The vast majority of commercial solar cells are made of crystalline silicon and therefore also different approaches were investigated to equip silicon surfaces with ‘moth-eye’ structures. For example, Sun et al. [113] developed a process to directly transfer the subwavelength structure into the substrate material. Therefore, they utilized a two-dimensional colloidal crystal as a shadow mask to generate a metallic nanohole array, which was exposed to an anisotropic wet-etching process leading to the formation of inverted pyramid arrays in silicon. In a different approach, Huang et al. [114] used self-assembled nanosphere lithography followed by photoassisted electrochemical etching to texturize the surface of silicon wafers with subwavelength structures possessing a high aspect ratio. In general, direct structuring of the silicon surface involves a cost-intensive etching process. An alternative is to place an antireflection large-area low-cost moth-eye film on top of the crystalline silicon photovoltaic modules that can be achieved using, e. g., a roll-to-roll process [115]. For moth-eye structures made of acrylic resin and coated on top of a silicon solar cell an increased electric generation of up to 15% was observed, depending on the incident angle [116]. A further approach of subwavelength structures on top of silicon solar cells involves a three-layer graded-index coating in which the final top layer consists of nanostructured silica that is deposited by an oblique-angle evaporation technique [117]. Here, an increase in the efficiency of more than 30% was observed compared to the untreated surface.

Also, solar cells other than silicon-based ones are covered with ‘moth-eye’ structures to reduce the surface reflection losses. In particular, GaAs solar cells have been highlighted due to their high efficiency, compared with conventional Si-based solar cells, which makes them ideal for space applications. In one approach glancing-angle deposition has been employed for preparing indium tin oxide (ITO) nanocolumns serving as a conductive AR layer for GaAs solar cells [118]. Here, for both s- and p-polarizations, omnidirectional and broadband AR characteristics are observed up to an incidence angle of 70° for the 350–900 nm wavelength range. Furthermore, GaAs solar cells have been fabricated by a combination of nanosphere lithography and subsequent reactive ion etching [119]. Hereby, the average reflectance of the ‘moth-eye’ textured GaAs surface was reduced from the initially 35.1% to 0.6% over a spectral range from 200 nm to 800 nm. In a similar procedure gallium antimonide (GaSb) substrates are also structured for thermophotovoltaic applications [120]. ‘Moth-eye’ structures were also used to increase the efficiency of high-temperature

thermopile infrared radiation sensors [121] and UV-sensitive silicon carbide photodetectors [122].

Another application of ‘moth-eye’ structures in optoelectronic devices are light-emitting diodes (LEDs). The quality of LEDs is directly influenced by the light extraction efficiency. Poor light-extraction properties may be due to total internal reflection (TIR) at the boundaries between the semiconductor materials and the outer air. Photons trapped inside the LED by TIR are converted to heat so that only a limited number of photons escape from the LED device to the air. To overcome these limitations subwavelength structures at the output surface are also applied. Kasugai et al. [123] developed a nitride-based blue LED with a moth-eye structure on the back of a 6H-SiC substrate that was textured by reactive ion etching. Here, the light-extraction efficiency and corresponding output power have been increased by a factor of 3.8 compared to a LED with a conventional structure. In an alternative procedure moth-eye structures were manufactured on a p-GaN top cladding layer by UV imprint and a following inductively coupled plasma etch process [124]. The transmittance of the moth-eye structured LED stacks was increased up to 1.5–2.5 times, compared to an identical unstructured LED sample. For commercialization, cost-effective fabrication techniques for producing such subwavelength structures are necessary. Here, Rao et al. [125] developed a promising embossing technology based on a h-PDMS mold that was subsequently used to transfer the nanostructure on the output surface of a In-GaAlP/GaAs red light-emitting diode by soft embossing. The manufactured devices showed an efficiency that was enhanced by 36% compared to the corresponding nonpatterned LED.

6. Conclusions

Specular reflection of light is a crucial issue both for animal vision in nature and in man-made optical systems. Bionics provides, on the one hand, the ‘technical’ solution, like on the eyes of a moth, to suppress these reflections and, on the other hand, bionics also provides self-optimized processes to realize this solution, which also can be transferred to industrial manufacturing technologies.

The biomimetic principle of the moth eye has already been discovered a few decades ago and since then a lot of progress has been made both in terms of theoretical understanding and fabrication technologies.

We have presented and discussed two distinct manufacturing techniques, the top-down approach and the bottom-up approach. The latter is more advantageous for curved and micro-optical surfaces, where interference lithography becomes difficult. Nonetheless, both manufacturing techniques have been successfully applied to modern industrial optical devices, such as high-performance photo-objectives, flat-panel displays and optical devices that rely on mass production of polymer optical components.

Despite the advantages, such as broadband applicability and higher angle-of-incidence tolerance, that moth-eye structures offer for high-performance optical components

and devices as presented in this paper, the number of applications, where they are actually used as anti-reflective layer, are still limited today. The reason is – as often in bionics and biomimetic concepts – that it is quite a challenge to catch up with nature’s evolutionary advance of some million years within only a few years of technical development. One of the obstacles so far has been the requirement for subwavelength distances between the individual structures. Until recently this had required the use of sophisticated and very costly lithographic techniques. But driven by the recent progress in the development of simulation tools and based on the strong improvements in manufacturing technologies of subwavelength structures, biomimetic antireflection structures, at last, now begin to leave the laboratory and become available for a broader range of applications.

There still remain some issues that make it unlikely that the moth-eye principle will replace classical layer-based coatings completely. Although moth-eye structured elements can be used over a broad thermal range since they are essentially free of adhesion problems and tensile stress between the substrate and the antireflection layer, they are somewhat sensitive to direct contact, e. g. fingerprints, or cleaning processes. Quite contrary to common belief, they show remarkable tolerance against mechanical stress and yet they are prone to contamination by dirt and cannot easily be cleaned by wiping. In fact, wiping anti-reflective moth-eye surfaces with a cloth results, of course, in cloth tatters between the otherwise intact protrusions, which are then difficult to remove. This contamination may reduce the optical performance drastically. Therefore, the antireflection structures are preferably found on inner surfaces, like for car-panel displays, and, on the outer surface, layer coatings are preferred.

The replicating technologies of nanostructures in polymers with an embossing or injection-molding process is also not trivial, as strong adhesion forces are likely to occur during the deforming step, which will negatively influence the lifetime of the mold. Additionally, many polymer applications are exposed to heavy mechanical stress (e. g. display covers) and under these difficult conditions the nanostructures are ultimately affected over time and show reduced performance. However, in our opinion, the advantages of anti-reflective coatings based on the moth-eye principle are manifold and, due to the impressive progress, which has been achieved in the last few years, the number of applications using this biomimetic principle has and will increase constantly. In particular, high-performance optics could gain significantly by an anti-reflective coating, which offers a higher angle-of-incidence tolerance and, therefore, allows for a higher transmittance of optical elements, like lenses with strong curvature.

Similar arguments hold for applications involving very high light intensities, as in various laser applications, or requiring a broad wavelength range, e. g., in optical spectrometry or fluorescent microscopy with different wavelengths. But in the near future classical anti-reflective coatings based on thin layers will most likely remain a competing technology for many applications. Thin-film coatings have been extensively used for more than 50 years now. They are

extremely well understood and there exist a variety of sophisticated manufacturing processes. As soon as the main issues concerning anti-reflective moth-eye structures, such as cheap manufacturing, easy cleanability and mechanical stability are solved, this million-year-old principle shall face a bright future.

Acknowledgements. We would like to thank all our scientific partners for their valuable cooperation and generous support. In particular, we express our acknowledgements to Takeharu Okuno (Canon, Utsunomiya-shi, Japan), Ulrike Schulz and Norbert Kaiser (both Fraunhofer IOF, Jena, Germany), Volkmar Boerner (Holo-tools, Freiburg, Germany), Andreas Gombert and Benedikt Bläsi (Fraunhofer ISE, Freiburg, Germany), and Hans Lauth (Fresnel Optics, Apolda, Germany). We also thank Dr. Michael Helgert and Matthias Burkhardt from Carl Zeiss Jena GmbH for their scientific support. This work was granted by the BMBF (project EFFET, contract no. 13N9713, and project PhoNa, contract no. 03IS2101E) and supported by the Max Planck Society.

Received: 17 February 2011, **Revised:** 16 September 2011,
Accepted: 16 September 2011

Published online: 29 November 2011

Key words: Micro- and nanostructured optics, manufacturing technologies, top-down and bottom-up lithography, subwavelength structuring, moth-eye structures, self-assembly, bionics and biomimetic concepts.



Robert Brunner received his Ph. D. degree in the field of near-field optical microscopy. After a postdoc visit at the University of Illinois, Urbana-Champaign he began in 1998 to work for the Research Center of the Carl-Zeiss company in Jena, Germany. Between 2001 and 2009 he was the responsible Lab Manager for Microstructured Optics of the Carl-Zeiss Technology Center. Since 2010 he holds

the chair for applied optics at the University of Applied Sciences in Jena. His current research interests are hybrid diffractive/refractive optics, subwavelength structures, refractive micro-optics, interference lithography and high-resolution optics.



Oliver Sandfuchs studied physics at Darmstadt University of Technology (Germany) and the University of California at Santa Cruz (USA) with the focus on nonlinear optics and nonlinear dynamical systems. In 2001 he received his Ph. D. in the field of spatiotemporal pattern formation and Fourier control in nonlinear optical feedback systems. Since 2002 he has worked at the Carl Zeiss, research and technology division in Jena. His current scientific interests are the design and manufacturing of micro- and nanooptical elements and bionic concepts in optoelectronics.



Claudia Pacholski received her Ph. D. in physical chemistry from the University of Hamburg, Germany, in 2002 working on the synthesis and self-assembly of semiconductor nanoparticles. She went on to do a postdoc at the University of California, San Diego from 2004 to 2006 focusing on the fabrication of optical biosensors based on porous silicon. Since 2007 she has been group leader at the Max Planck

Institute for Metals Research in Stuttgart, Germany. Her research areas include the chemical synthesis and fabrication of nanomaterials by exploiting self-assembly leading to nanomaterials with optical properties that can find application in optical devices.



Christoph Morhard studied physics in Ulm and Heidelberg (Germany). After a short stay at the MPI for Nuclear Physics (Heidelberg) he moved in 2008 to the MPI for Metals Research in Stuttgart. He received his PhD in physics from the University of Heidelberg (2010) for his work in Stuttgart on the nanostructuring of surfaces. He is currently working as a postdoc at the MPI for Metals Research. His

research area is the use of bottom-up technologies to fabricate surfaces structured on the nanoscale and especially the development of superior anti-reflective coatings close to the market.



Joachim Spatz received his Ph. D. from Ulm University in 1996. Between 1997 and 1998 he worked as a postdoc at the Institut Curie in Paris in the area of cellular biophysics. In 2000 he was awarded the *venia legendi* ('Habilitation') in Physics at Ulm University and in October 2000 he accepted an appointment for a Professorship in Biophysical Chemistry at the University of Heidelberg. Since 2003 he is

also an Adjunct Senior Faculty Member at the Jackson Laboratory, ME, USA. Since October 2004 he is a Scientific Member and Director at the Max Planck Institute for Metals Research while, at the same time, holding a secondary appointment as Professor for Biophysical Chemistry at the University of Heidelberg. Since 2007 he is Acting Director of the Max Planck Institute for Metals Research.

References

- [1] W. Nachtigall, *Bionik – Grundlagen und Beispiele für Ingenieure und Naturwissenschaftler* (Springer, Berlin, 2002).
- [2] C. Darwin, *The Origin of Species* (John Murray, London, 1859).
- [3] J. R. Sheats and B. W. Smith, *Microolithography – Science and Technology* (Marcel Dekker, New York, 1998).
- [4] M. F. Land and D. E. Nilsson, *Animal Eyes* (Oxford University Press Inc, New York, 2002).

- [5] D. Attwood, *Soft X-Ray and Extreme Ultraviolet Radiation – Principles and Applications* (Cambridge University Press, Cambridge, UK, 1999).
- [6] G. D. Bernard and W. H. Miller, *Investigative Ophthalmology* **7**, 416–434 (1969).
- [7] A. R. Parker, *In the Blink of an Eye* (Cambridge University Press, Mass., 2003).
- [8] L. P. Biro and J.-P. Vigneron, *Laser Photon. Rev.* **5**, 27–51 (2011).
- [9] B. Berge and J. Peseux, *Eur. Phys. J. E* **3**, 159–163 (2000).
- [10] D. Y. Zhang, N. Justis, and Y. H. Lo, *Opt. Commun.* **249**, 175–182 (2005).
- [11] A. Weber and H. Zappe, *Appl. Opt.* **44**, 3238–3245 (2005).
- [12] Ph. Ball, *The Self-Made Tapestry: Pattern Formation in Nature* (Oxford University Press, New York, 1999).
- [13] S. Johnson, *Sci. Am.* **2**, 80–89 (2000).
- [14] C. G. Bernhard, *Endeavour* **26**, 79–84 (1967).
- [15] P. B. Clapham and M. C. Hutley, *Nature* **244**, 281–282 (1973).
- [16] F. Träger, (ed.), *Advanced Optical Components*, Springer Handbook of Lasers and Optics (Springer, New York, 2007), Chap. 8.
- [17] A. R. Parker, *Philos. Trans. R. Soc. Lond. A* **362**, 2709–2720 (2004).
- [18] D. Malacara, *Optical Shop Testing*, 2nd edn, (John Wiley & Sons, Canada, 2007).
- [19] C. M. Horwitz, *Opt Commun.* **11**, 210–212 (1974).
- [20] R. C. McPhedran and D. Maystre, *Appl Phys.* **14**, 1–20 (1977).
- [21] L. H. Cescato, E. Gluch, and N. Streibl, *Appl. Opt.* **29**, 3286–3290 (1990).
- [22] I. Richter, P.-Ch. Sun, F. Xu, and Y. Fainman, *Appl. Opt.* **34**, 2421–2429 (1995).
- [23] I. Richter, P.-Ch. Sun, F. Xu, and Y. Fainman, *Proc. SPIE* **2404**, 69–80 (1995).
- [24] R.-Ch. Tyan, P.-Ch. Sun, and Y. Fainman, *Proc. SPIE* **2689**, 82–89 (1996).
- [25] R.-Ch. Tyan, A. A. Salvekar, H.-P. Chou, Ch.-Ch. Cheng, A. Scherer, P.-Ch. Sun, F. Xu, and Y. Fainman, *J. Opt. Soc. Am. A* **14**, 1627–1636 (1997).
- [26] P. Lalanne, J. Hazart, P. Chavel, E. Cambril, and H. Launois, *J. Opt. A, Pure Appl. Opt.* **1**, 215–219 (1999).
- [27] H. Haidner, P. Kipfer, W. Stork, and N. Streibl, *Optik* **89**, 107–112 (1992).
- [28] M. W. Farn, *Appl. Opt.* **31**, 4453–4458 (1992).
- [29] M. Collischon, H. Haidner, P. Kipfer, A. Lang, J. T. Sheridan, J. Schwider, N. Streibl, and J. Lindolf, *Appl. Opt.* **33**, 3572–3577 (1994).
- [30] P. Lalanne, S. Astilean, P. Chavel, E. Cambril, and H. Launois, *Opt. Lett.* **23**, 1081–1083 (1998).
- [31] J. N. Mait, D. W. Prather, and M. S. Mirotznik, *Opt. Lett.* **23**, 1343–1345 (1998).
- [32] A. Mizutani, H. Kikuta, K. Iwata, and H. Toyota, *J. Opt. Soc. Am. A* **19**, 1346–1351 (2002).
- [33] M. Karlsson and F. Nikolajeff, *Opt. Express* **11**, 502–507 (2003).
- [34] Y. Zhao, J. Wang, and G. Mao, *Opt. Lett.* **30**, 1885–1887 (2005).
- [35] R. Leitel, U. Schulz, N. Kaiser, and A. Tünnermann, *Appl. Opt.* **47**, C143–C146 (2008).
- [36] Fraunhofer Institut für Solare Energiesysteme, Freiburg, Germany, www.ise.fraunhofer.de, last visited December 2010.
- [37] Fresnel Optics GmbH, Apolda, Germany, www.fresnel-optics.de, last visited December 2010.
- [38] Holotools GmbH, Freiburg, Germany, www.holotools.de, last visited December 2010.
- [39] U. Schulz, C. Präfke, C. Gödeker, N. Kaiser, and A. Tünnermann, *Appl. Opt.* **50**, C31–C35 (2011).
- [40] U. Schulz, P. Munzert, R. Leitel, I. Wendling, N. Kaiser, and A. Tünnermann, *Opt. Express* **15**, 13108–13113 (2007).
- [41] J. P. Spatz, *Angew. Chem. Int. Ed.* **114**, 3359 (2002).
- [42] C.-H. Sun, B. J. Ho, B. Jiang, and P. Jiang, *Opt. Lett.* **33**, 2224–2226 (2008).
- [43] S. Chattopadhyay, Y. F. Huang, Y. J. Yen, A. Ganguly, K. H. Chen, and L. C. Chen, *Mater. Sci. Eng. R* **69**, 1–35 (2010).
- [44] Y. Li, J. Zhang, and B. Yang, *Nano Today* **5**, 117–127 (2010).
- [45] E. Hecht, *Optics*, 4th edn. (Addison Wesley, San Francisco, 2002), Chap. 4.
- [46] S. J. Wilson and M. C. Hutley, *Opt. Acta* **7**, 993–1009 (1982).
- [47] H. G. Shanhogue, C. L. Nagendra, M. N. Annapurna, S. Ajith Kumar, and G. K. M. Thutupalli, *Appl. Opt.* **36**, 6339–6351 (1997).
- [48] U. Schulz, *Opt. Express* **17**, 8704–8708 (2009).
- [49] S. Kawakami, O. Hanaizumi, T. Sato, Y. Ohtera, T. Kawashima, N. Yasuda, Y. Takei, and K. Miura, *Electron. Commun. Jpn. 2, Electron. (USA)* **82**, 43–52 (1999).
- [50] O. Sandfuchs, D. Pätz, S. Sinzinger, A. Pesch, and R. Brunner, *J. Opt. Soc. Am. A* **25**, 1885–1893 (2008).
- [51] M. A. Golub and A. A. Friesem, *J. Opt. Soc. Am. A* **24**, 687–695 (2007).
- [52] O. Sandfuchs, C. Schwanke, M. Burkhardt, F. Wyrowski, A. Gatto, and R. Brunner, *J. Eur. Opt. Soc.* **5**, 10059–10068 (2010).
- [53] R. Haïdar, G. Vincent, N. Guérineau, S. Collin, S. Velghe, and J. Primot, *Opt. Express* **13**, 9941 (2005).
- [54] S. A. Boden and D. M. Bagnall, *Appl. Phys. Lett.* **93**, 133108–133110 (2008).
- [55] P. Lalanne and D. Lemerrier-Lalanne, *J. Mod. Opt.* **43**, 2063–2086 (1996).
- [56] W. H. Southwell, *J. Opt. Soc. Am. A* **8**, 549–553 (1991).
- [57] D. H. Raguin and G. M. Morris, *Appl. Opt.* **32**, 1154–1167 (1993).
- [58] D. Lehr, M. Helgert, M. Sundermann, Ch. Morhard, C. Pacholski, J. Spatz, and R. Brunner, *Opt. Express* **18**, 23878–23890 (2010).
- [59] F. T. Chen and H. G. Craighead, *Opt. Lett.* **20**, 121–123 (1994).
- [60] Z. Zhou and T. J. Drabik, *J. Opt. Soc. Am. A* **12**, 1104–1112 (1995).
- [61] M. E. Motamedi, W. H. Southwell, and W. J. Gunning, *Appl. Opt.* **31**, 4371–4376 (1992).
- [62] A. Cornu, *C. R. Acad. Paris* **80**, 645–649 (1875).
- [63] N. K. Sheridan, *Appl. Phys. Lett.* **12**, 316–318 (1968).
- [64] A. Labeyrie, *Elect. Opt. Syst. Des.* **2**, 32–38 (1971).
- [65] E. G. Loewen and E. Popov, *Diffraction Gratings and Applications* (Marcel Dekker, New York, 1997).
- [66] R. Brunner, M. Burkhardt, N. Correns, and K. Rudolf, *Opt. Express* **16**, 12239–12250 (2008).
- [67] S. J. Wilson and M. C. Hutley, *Opt. Acta* **29**, 993–1009 (1982).

- [68] A. Gombert, K. Rose, A. Heinzl, W. Horbelt, Ch. Zanke, B. Bläsi, and V. Wittwer, *Sol. Energy Mater. Sol. Cells* **54**, 333–342 (1998).
- [69] A. Gombert and B. Bläsi, in: *Functional Properties of Bio-Inspired Surfaces*, edited by E. A. Favret and N. O. Fuentes (World Scientific Publishing, Singapore, 2009), pp. 79–102.
- [70] P. Lalanne, *J. Opt. Soc. Am. A* **16**, 2517–2520 (1999).
- [71] G. Vincent, R. Haidar, S. Collin, N. Guerneau, J. Primot, E. Cambriil, and J.-L. Pelouard, *J. Opt. Soc. Am. B* **25**, 834–840 (2008).
- [72] D. Chen, *Sol. Energy Mater. Sol. Cells* **68**, 313–336 (2001).
- [73] P. K. Biswas, D. Kundu, and D. Ganguli, *J. Mater. Sci. Lett.* **8**, 1436–1437 (1989).
- [74] C. J. Brinker and M. S. Harrington, *Sol. Energy Mater.* **5**, 159–172 (1981).
- [75] M. Faustini, L. Nicole, C. Boissire, P. Innocenzi, C. Sanchez, and D. Grosso, *Chem. Mater.* **22**, 4406–4413 (2010).
- [76] F. Guillemot, A. Brunet-Bruneau, E. Bourgeat-Lami, T. Gacoin, E. Barthel, and J.-P. Boilot, *Chem. Mater.* **22**, 2822–2828 (2010).
- [77] K. Haas, S. Amberg-Schwab, K. Rose, and G. Schottner, *Surf. Coat. Technol.* **111**, 72–79 (1999).
- [78] T. Okuno, *Proc. SPIE* **7652**, 765203–1 (2010).
- [79] S.-M. Yang, S. G. Jang, D. G. Choi, S. Kim, and H. K. Yu, *Small* **2**, 458–475 (2006).
- [80] J. H. Zhang and B. Yang, *Adv. Funct. Mater.* **20**, 3411–3424 (2010).
- [81] A. S. Dimitrov and K. Nagayama, *Langmuir* **12**, 1303–1311 (1996).
- [82] B. G. Prevo, D. M. Kuncicky, and O. D. Velev, *Colloids Surf. A* **311**, 2–10 (2007).
- [83] H. L. Chen, S. Y. Chuang, C. H. Lin, and Y. H. Lin, *Opt. Express* **15**, 14793–14803 (2007).
- [84] Y. Li, F. Liu, and J. Q. Sun, *Chem. Commun.* **19**, 2730–2732 (2009).
- [85] H. B. Xu, N. Lu, D. Qi, J. Hao, L. Gao, B. Zhang, and L. Chi, *Small* **4**, 1972–1975 (2008).
- [86] Y. F. Li, J. H. Zhang, and B. Yang, *Langmuir* **26**, 9842–9847 (2010).
- [87] X. M. Zhang, J. H. Zhang, Z. Y. Ren, X. Li, X. Zhang, D. Zhu, T. Wang, T. Tian, and B. Yang, *Langmuir* **25**, 7375–7382 (2009).
- [88] D. G. Stavenga, S. Foletti, G. Palasantzas, and K. Arikawa, *Proc. Roy. Soc. B* **273**, 661–667 (2006).
- [89] P. Jiang, *Langmuir* **22**, 3955–3958 (2006).
- [90] W. L. Min, B. Jiang, and P. Jiang, *Adv. Mater.* **20**, 3914 (2008).
- [91] W. L. Min, P. Jiang, and B. Jiang, *Nanotechnology* **19**, 475604–475610 (2008).
- [92] C. H. Sun, P. Jiang, and B. Jiang, *Appl. Phys. Lett.* **92**, 061112–061114 (2008).
- [93] T. Lohmüller, M. Helgert, M. Sundermann, R. Brunner, and J. P. Spatz, *Nano Lett.* **8**, 1429–1433 (2008).
- [94] C. Morhard, C. Pacholski, D. Lehr, R. Brunner, M. Helgert, M. Sundermann, and J. P. Spatz, *Nanotechnology* **21**, 425301 (2010).
- [95] G. Kästle, H.-G. Boyen, F. Weigl, G. Lengl, T. Herzog, P. Ziemann, S. Riethmüller, and O. Mayer, *Adv. Funct. Mater.* **13**, 853–861 (2003).
- [96] R. Glass, M. Moller, and J. P. Spatz, *Nanotechnology* **14**, 1153–1160 (2003).
- [97] K. Tsujino, M. Matsumura, and Y. Nishimoto, *Sol. Energy Mater. Sol. Cells* **90**, 100–110 (2006).
- [98] S. J. Park, S. W. Lee, K. J. Lee, J. H. Lee, K. D. Kim, J. H. Jeong, and J. H. Choi, *Nanoscale Res. Lett.* **5**, 1570–1577 (2010).
- [99] J. Y. Hao, J. Y. Hao, N. Lu, H. B. Xu, W. T. Wang, L. G. Gao, and L. F. Chi, *Chem. Mater.* **21**, 1802–1805 (2009).
- [100] D. Qi, N. Lu, H. Xu, B. Yang, and C. Huang, *Langmuir* **25**, 7769–7772 (2009).
- [101] Y.-J. Lee, D. S. Ruby, D. W. Peters, B. B. McKenzie, and J. W. P. Hsu, *Nano Lett.* **8**, 1501–1505 (2008).
- [102] M. K. Kim, D. K. Yi, and U. Paik, *Langmuir* **26**, 7552–7554 (2010).
- [103] H. Gao, Z. Liu, J. Zhang, G. Zhang, and G. Xie, *Appl. Phys. Lett.* **90**, 123115 (2007).
- [104] H. Xu, N. Lu, G. Shi, D. Qi, B. Yang, H. Li, W. Xu, and L. Chi, *Langmuir* **27**, 4963–4967 (2011).
- [105] Y. M. Song, G. Ch. Park, S. J. Jang, J. H. Ha, J. S. Yu, and Y. T. Lee, *Opt. Express* **19**, A157–A165 (2011).
- [106] A. Disch, J. Mick, B. Bläsi, and C. Müller, *Microsyst. Technol.* **13**, 483–486, (2007).
- [107] S. S. Oh, Ch.-Gi Choi, and Y.-S. Kim, *Microelectron. Eng.* **87**, 2328–2331, (2010).
- [108] A. Gombert and H. Lerchenmüller, Antireflective coating and method of manufacturing same, Patent US 6,359,735 B1.
- [109] V. Boerner, Holographic antiglare and antireflection films for flat panel displays, in: *Proceedings of the SID International Symposium (Baltimore, USA, 2003)*, pp. 68–71.
- [110] MacDermid Autotype Inc., Denver, Colorado, USA, www.macdermidautotype.com, last visited December 2010.
- [111] A. Kaless, U. Schulz, P. Munzert, and N. Kaiser, *Surf. Coat. Technol.* **200**, 58–61 (2005).
- [112] U. Schulz, P. Munzert, N. Bollwahn, and N. Kaiser, *Chinese Opt. Lett.* **8**, 177–179 (2010).
- [113] Ch.-H. Sun, W.-L. Min, N. C. Linn, and P. Jianga, *Appl. Phys. Lett.* **91**, 231105 (2007).
- [114] M.-J. Huang, Ch.-R. Yang, Y.-Ch. Chiou, R.-T. Lee, *Solar Energy Mater. Solar Cells* **92**, 1352–1357 (2008).
- [115] N. Yamada, T. Ijiri, E. Okamoto, K. Hayashi, and H. Masuda, *Opt. Express* **19**, A118–A125 (2011).
- [116] N. Yamada, O. N. Kim, T. Tokimitsu, Y. Nakai, and H. Masuda, *Prog. Photovolt, Res. Appl.* **19**, 134–140 (2011).
- [117] S. Chhahjed, M. F. Schubert, J. K. Kim, and E. F. Schubert, *Appl. Phys. Lett.* **93**, 251108 (2008).
- [118] P. Yu, Ch.-H. Chang, Ch.-H. Chiu, Ch.-Sh. Yang, J.-Ch. Yu, H.-Ch. Kuo, Sh.-H. Hsu, and Y.-Ch. Chang, *Adv. Mater.* **21**, 1618–1621 (2009).
- [119] B.-J. Kim and J. Kim, *Opt. Express* **19**, A326–A330 (2011).
- [120] W.-L. Min, A. P. Betancourt, P. Jiang, and B. Jiang, *Appl. Phys. Lett.* **92**, 141109 (2008).
- [121] T. Glaser, A. Ihring, W. Morgenroth, N. Seifert, S. Schröter, and V. Baier, *Microsystem Technol.* **11**, 86–90 (2005).
- [122] Y. Hirabayashia, S. Kaneko, K. Akiyama, M. Yasui, and K. Sakurazawa, *Mater. Sci. Forum* **645–648**, 1073–1076 (2010).
- [123] H. Kasugai, Y. Miyake, A. Honshio, Sh. Mishima, T. Kawashima, K. Iida, M. Iwaya, S. Kamiyama, H. Amano, I. Akasaki, H. Kinoshita, and H. Shiomi, *Jpn. J. Appl. Phys.* **44**, 7414–7417 (2005).
- [124] E.-J. Honga, K.-J. Byeona, H. Parka, J. Hwanga, H. Leea, K. Choib, and G. Y. Jung, *Mater. Sci. Eng. B* **163**, 170–173, (2009).
- [125] J. Rao, R. Winfield, and L. Keeney, *Opt. Commun.* **283**, 2446–2450, (2010).